AD-A053 904 LEHIGH UNIV BETHLEHEM PA INST OF FRACTURE AND SOLID --ETC F/G 11/6
LOAD AND ENVIRONMENT INTERACTIONS IN FATIGUE CRACK GROWTH UNDER--ETC(U)
JAN 78 R P WEI AFOSR-75-2857
UNCLASSIFIED IFSM-78-88 AFOSR-TR-78-0788 NL

| OF |
AD A
053904

END
DATE
FILMED
6-78
DDC

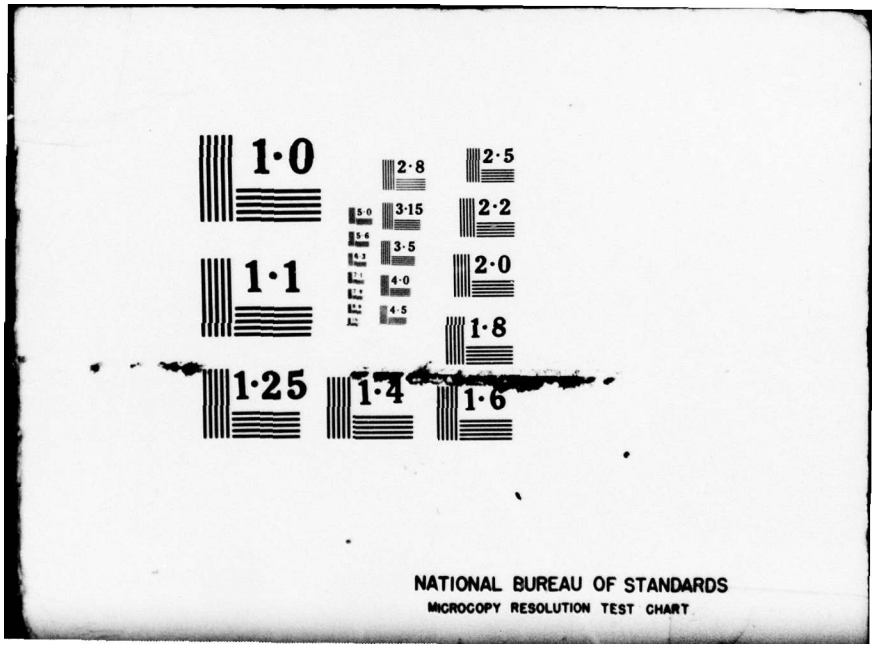
1·0
1·1
1·25
1·4
1·6
1·8
2·0
2·2
2·5
2·8
3·15
3·5
4·0
4·5
5·0
NATIONAL BUREAU OF STANDARDS
MICROCOPY RESOLUTION TEST CHART

INSTITUTE OF FRACTURE AND SOLID MECHANICS

IPSM-78-88

(2)

LEHIGH UNIVERSITY

LOAD AND ENVIRONMENT INTERACTIONS IN FATIGUE CRACK GROWTH UNDER SPECTRUM LOADING

by

R. P. Wei

January 1978

Final Report

Air Force Office of Scientific Research

Grant No. AFOSR-75-2857

Qualified requestors may obtain additional copies from the Defense Documentation Center, all others should apply to the National Technical Information Service.

AIR FORCE OFFICE OF SCIENTIFIC RESEARCH (AFSC)
NOTICE OF TRANSMITTAL TO DDC
This technical report has been reviewed and is approved for public release IAW AFR 190-12.
Distribution is unlimited.
A. D. BLOSE
Technical Information Officer

Final Report
To The Air Force Office of Scientific Research

LOAD AND ENVIRONMENT INTERACTIONS IN FATIGUE CRACK GROWTH UNDER SPECTRUM LOADING

by

R. P. Wei
LEHIGH UNIVERSITY
Bethlehem, Pennsylvania U.S.A.

January, 1978

Research sponsored by the Air Force Office of Scientific Research, Air Force Systems Command, USAF, under Grant No. AFOSR-75-2857. The United States Government is authorized to reproduce and distribute reprints for Governmental purposes notwithstanding any copyright notation hereon.

LOAD AND ENVIRONMENT INTERACTIONS IN FATIGUE CRACK GROWTH UNDER SPECTRUM LOADING

AFOSR-75-2857

by

R. P. Wei
LEHIGH UNIVERSITY
Bethlehem, Pennsylvania 18015

SUMMARY

The importance of delay (or, retardation in the rate of fatigue crack growth) produced by load interactions in variable-amplitude loading on the accurate prediction of fatigue lives of aircraft and other engineering structures has been recognized for some time and has begun to receive greater attention in recent years. Recent investigations showed that the effects of delay can be quite large, and that these effects need to be taken into account in developing improved fatigue analysis procedures for aircraft and other engineering structures.

A number of models (based on the concepts of crack closure, residual stress intensity factor, etc.) have been proposed to account for the effects of delay. These models, while successfully predicting trends in the rate of fatigue crack growth for randomized load spectra, appear to break down for ordered spectra. Several basic problems contributed to the lack of complete success, and needs to be resolved in the development of improved models for predicting load interaction effects (chiefly delay) on fatigue crack growth. They are:

- o Proper characterization and physical understanding of the complex phenomena of crack acceleration and delay associated with changes in load level, and of the effects of thermal and chemical environments on these phenomena.
- o Adequate description of crack tip stress intensity factors to account for various types of loading, crack geometry and residual stresses.
- o Proper description of the kinetics of fatigue crack growth under constant-amplitude loading, including the effects of stress ratio, cyclic load frequency and service environment, and assessment of variability in these kinetic data.

To address some of the issues, the following three investigations were carried out under this grant:

(1) Experimental evaluation of crack closure and its viability as a model for describing fatigue crack growth kinetics and delay.

(2) Examinations of the influences of plate thickness, K level and chemical environment on fatigue crack growth response following a single high-load excursion (overload) to develop further phenomenological understanding of load interaction effects in fatigue.

(3) Assessment of the contributions of crack length measurement interval and precision, and data processing procedures on variability to provide background for interpretation of experimental data on fatigue crack growth kinetics and their utilization in life prediction.

2219-T851 aluminum alloy plates were used in the first two investigations. Computer simulation was used in the last investigation to preclude all other variables. Results from the first

investigation have been included in an Interim Report, entitled "Crack Closure and Fatigue Crack Growth in 2219-T851 Aluminum Alloy", by K. D. Unangst, T. T. Shih and R. P. Wei, dated August 1976 (AFOSR-TR-76-1247, ADA633082). The principal results have been reported also in a technical publication, entitled "Crack Closure in 2219-T851 Aluminum Alloy", by the same authors in the Journal of Engineering Fracture Mechanics (v. 9, 1977, pp. 725-734). Results from the other two investigations have been prepared in the form of technical publications and are included here as Appendices A and B. Brief summaries of these investigations are given here.

The effects of specimen thickness, stress ratio (R) and maximum stress intensity factor (K_{max}) on crack closure (or opening) and on fatigue crack growth kinetics were studied using a 2219-T851 aluminum alloy. The crack length and the occurrence of crack closure were measured by an electrical potential method. The experimental work was carried out within the framework of linear-elastic fracture mechanics. The experimental results show that the onset of crack closure (or opening) depends on R, K_{max}, and specimen thickness. In terms of the "effective stress intensity range ratio" (U), as defined by Elber, the results show that U tends to increase for increasing R, decrease for increasing K_{max}, and decrease with increasing specimen thickness. From these trends, it is shown that the "effective stress intensity range" (ΔK_{eff}) does not always increase with increasing stress intensity range (ΔK). The fatigue crack growth data show that the specimen thickness does not have a significant effect on crack growth in

this material over the lower crack growth rate region; below about 5×10^{-6} in./cycle (1.3×10^{-5}) cm/cycle). In the higher crack growth rate region, above about 5×10^{-6} in./cycle (1.3×10^{-5} cm/cycle), the crack growth rates are higher for the thicker specimens. The viability of the crack closure model is questioned. The experimenal results show that crack closure cannot fully account for the effects of stress ratio and specimen thickness or K_{max} on fatigue crack growth. The use of ΔK_{eff} as a parameter for characterizing the mechanical driving force for fatigue crack growth is questioned.

To develop further phenomenological understanding of load interaction effects in fatigue, examinations of the influences of plate thickness, stress intensity (K) level and chemical environment on fatigue crack growth response following a single high-load excursion (overload) were carried out on a 2219-T851 aluminum alloy. An overload ratio (that is, the ratio between the magnitude of the overload and the maximum in the subsequent constant-amplitude fatigue loading) of 2.0 was used. Experiments were carried out in dehumidified argon, air, and 3.5 pct NaCl solution at room temperature. The results showed that delay (as measured by the duration of overload affected crack growth) increased with decreasing plate thickness and with increasing K level, and decreased with increasing aggressiveness of the chemical environment.

The high-load excursion (overload) affected crack growth through a region of material ahead of the crack tip. Within this overload affected zone, crack growth rate first increased (some-

times), followed by fairly rapid decrease to a minimum value (delayed retardation), and then increased gradually to its steady-state value. The overload affected zone size was found to depend on crack-tip constraint and to be independent of chemical environment, and was found to be equal to the appropriate (plane-strain or plane-stress) plastic zone size for the overload. Identification of a delayed retardation zone was made, and identification of this zone with the cyclic plastic zone size for the preceding fatigue loading was suggested. The effects of plate thickness, K level and chemical environment on delay were considered in relation to their respective influences on the overload-affected-zone and delayed-retardation-zone sizes, and on the rate of fatigue crack growth. A residual stress intensity concept for describing fatigue crack growth response within the overload affected zone was considered. With suitable modifications, reasonable estimates of crack growth response could be obtained. Further verification and understanding of these modifications are discussed.

A computer simulation of the primary fatigue crack growth data (crack length versus elapsed cycles or a versus N) was made to examine the influences of crack length measurement interval and precision, and of the associated data processing procedure on the resulting data on fatigue crack growth kinetics (i.e., da/dN versus ΔK). Variability in the derived growth rate (da/dN) data depended strongly on the magnitude of the measurement interval relative to the measurement precision. It was reduced by those data processing procedures (such as the incremental polynomial

methods) that fitted a smooth curve through portions of the primary data. Such procedures, however, introduced significant bias into the derived data on fatigue crack growth kinetics. The results further suggested that much of the variability in the published data on fatigue crack growth kinetics might be attributed to sources described herein. Caution is, therefore, recommended in attempting to draw statistical inferences regarding material variability from these data.

Results from these investigations have provided additional insignt into load and environment interactions in fatigue crack growth under variable-amplitude (spectrum) loading, as well as for fatigue under constant-amplitude loading. These results should be considered in assessing current and improved life prediction procedures.

APPENDIX A

FATIGUE CRACK GROWTH RESPONSE FOLLOWING A HIGH-LOAD EXCURSION IN 2219-T851 ALUMINUM ALLOY

FATIGUE CRACK GROWTH RESPONSE FOLLOWING A HIGH-LOAD EXCURSION IN 2219-T851 ALUMINUM ALLOY

by

R. P. Wei[1], N. E. Fenelli[1], K. D. Unangst[2] and T. T. Shih[3]
LEHIGH UNIVERSITY
Bethlehem, Pennsylvania 18015

ABSTRACT

To develop further phenomenological understanding of load interaction effects in fatigue, examinations of the influences of plate thickness, stress intensity (K) level and chemical environment on fatigue crack growth response following a single high-load excursion (overload) were carried out on a 2219-T851 aluminum alloy. An overload ratio (that is, the ratio between the magnitude of the overload and the maximum in the subsequent constant-amplitude fatigue loading) of 2.0 was used. Experiments were carried out in dehumidified argon, air, and 3.5 pct NaCl solution at room temperature. The results showed that delay (as measured by the duration of overload affected crack growth) increased with decreasing plate thickness and with increasing K level, and decreased with increasing aggressiveness of the chemical environment.

---

[1]R. P. Wei and N. E. Fenelli are Professor of Mechanics and Undergraduate Assistant respectively in the Department of Mechanical Engineering and Mechanics.

[2]K. D. Unangst, formerly Research Assistant in the Department of Mechanical Engineering and Mechanics, is now on assignment with the U. S. Navy.

[3]T. T. Shih, formerly Research Scientist with the Department of Mechanical Engineering and Mechanics, is affiliated with Westinghouse R & D Center, Pittsburgh, PA.

The high-load excursion (overload) affected crack growth through a region of material ahead of the crack tip. Within this overload affected zone, crack growth rate first increased (sometimes), followed by fairly rapid decrease to a minimum value (delayed retardation), and then increased gradually to its steady-state value. The overload affected zone size was found to depend on crack-tip constraint and to be independent of chemical environment, and was found to be equal to the appropriate (plane-strain or plane-stress) plastic zone size for the overload. Identification of a delayed retardation zone was made, and identification of this zone with the cyclic plastic zone size for the preceding fatigue loading was suggested. The effects of plate thickness, K level and chemical environment on delay were considered in relation to their respective influences on the overload-affected-zone and delayed-retardation-zone sizes, and on the rate of fatigue crack growth. A residual stress intensity concept for describing fatigue crack growth response within the overload affected zone was considered. With suitable modifications, reasonable estimates of crack growth response could be obtained. Further verification and understanding of these modifications are discussed.

INTRODUCTION

The importance of delay (retardation in the rate of fatigue crack growth), produced by load interaction in variable-amplitude loading, on the accurate prediction of fatigue lives of aircraft and other engineering structures has been well recognized for some time [1-6]. Several models have been proposed to account for the effects of delay in fatigue analysis of structures [7-15]. These models, while successfully predicting trends in the rate of fatigue crack growth for randomized load spectra, appear to break down (in most cases) for ordered spectra [6-18]. Development of improved models to account for the effects of delay, however, depends on a more complete understanding of the process of delay itself. Available systematic data for simple loading conditions (particularly for the Ti-6Al-4V alloy) indicate that delay in fatigue crack growth is a highly complex phenomenon, and can be affected by both chemical and thermal environments, as well as by section size (specifically plate thickness) [19-26]. To expand on the phemonenological understanding of delay, the effects of chemical environment, (dehumidified argon, air and 3.5 pct NaCl solution) stress intensity (K) level and plate thickness were investigated for fatigue crack growth following a single high-load excursion ("overload") in a 2219-T851 aluminum alloy at room temperature.

Delay properly refers to the period of abnormally low rate, or approximately zero rate, of fatigue crack growth between a decrease in load level and the establishment of a rate of crack growth commensurate with that for constant-amplitude loading at the

prevailing (lower) load; that is, between Points B and E in the schematic diagram shown in Figure 1. (Note that in Figure 1 the phenomena of crack acceleration and delayed retardation, that is, B to B' and B' to C, are also illustrated [19]). The response following a single high-load excursion (overload) is depicted here (see inset in Figure 1 where the loading parameter is given in terms of the crack-tip stress intensity factor K). Following Jonáš and Wei [21], subscripts 1 and 2 are used to denote parameters associated with the overload and the steady-state fatigue loads respectively.

Two of the current procedures used to define delay in terms of the number of elapsed cycles are illustrated in Figure 1a. In the first method, delay (N_D) is artificially defined as a period of zero crack growth, represented by the interval B'E' in Figure 1a, and is obtained by extrapolating the constant-amplitude growth curve (Curve EF) to E'. This definition of delay was used with considerable success for the Ti-6Al-4V alloy, since there was minimal crack acceleration and delayed retardation [19]. The alternative definition for delay includes the entire period affected by the high-load excursion, and delay (N_D^*) is depicted by the interval from B to E (see Figure 1a). A corresponding "overload affected zone" is defined in Figure 1b (Point B' to E) along with the detailed crack growth response.

Because of the occurrence of crack acceleration and delayed retardation in some of the aluminum alloys and to provide more detailed description of crack growth response, the second of these two procedures was implicitly adopted for this investigation.

Emphasis was placed, therefore, on examining the rate of fatigue crack growth as a function of crack extension and of elapsed cycles before and following a single high-load excursion (overload), see Figure 1. Experiments were carried out within the framework of linear fracture mechanics. The crack tip stress intensity factor K or ΔK was used to characterize the mechanical driving force for crack growth.

MATERIAL AND EXPERIMENTAL WORK

Material

A 7.6 cm (3 in.) thick plate[1] and a 1.65 cm (0.65 in.) thick plate[2] of 2219-T851 aluminum alloy were used in this study. Chemical composition and tensile properties for the 7.6 cm thick plate are given in Table 1[3].

Specimen and K Calibration

Wedge-opening-load (WOL) specimens, with half-height to width ratio (H/W) of 0.486, were selected for use in this study. The specimens were oriented in the longitudinal (LT) orientation. Two slightly different configurations were used to facilitate attachment of leads for the electrical-potential crack measurement system (see Figure 2). Specimens with thicknesses of 0.25, 0.51, 0.76 and 1.27 cm (0.1, 0.2, 0.3 and 0.5 in.) were machined from

(1) Plate supplied by Westinghouse Electric Corporation, and was a part of the material used in an AFML sponsored program (Contract F33615-75-C-5064) on fatigue crack growth.
(2) Plate furnished by AFFDL.
(3) Chemical composition and tensile properties were not determined on the 1.65 cm (0.65 in.) thick plate. They are expected, however, to be comparable to those for the 7.6 cm (3.0 in.) thick plate.

the 7.6 cm (3 in.) thick plate. These specimens conformed to dimensions shown in Figure 2a, and were randomized in the thickness direction. Specimens from the 1.65 cm (0.65 in.) thick plate were machined in accordance with Figure 2b, and were in full thickness. An initial (or crack starter) notch, 1.96 cm (0.77 in.) in length, was introduced into each specimen by electro-discharge machining (EDM). Each specimen was precracked in fatigue through a decreasing sequence of loads that terminated at the desired load level (or initial K) for the actual experiment. The precracking procedure provided a fatigue crack of about 0.33 cm (0.13 in.) in length from the starter notch, corresponding to a crack length of about 2.29 cm (0.9 in.) at the start of each experiment. This precracking procedure ensured that the subsequent fatigue crack growth would be through material that had not been altered by the notch preparation procedure, and would be unaffected by the starter notch geometry.

Stress intensity factor, K, for the WOL specimen was computed from Eq. 1 [27,28]:

$$K = \frac{P}{BW}\sqrt{a}\,[30.96 - 195.8\,(a/W) + 730.6\,(a/W)^2 - 1186.3\,(a/W)^3 + 754.6\,(a/W)^4] \quad (1)$$

P = applied load; B = specimen thickness; W = specimen width; and a = crack length. Both specimen width and crack length were measured from the line of loading, as shown in Figure 2.

Experimental Procedures

Fatigue crack growth experiments to study load interaction

effects were carried out in a closed-loop electrohydraulic testing machine operated in load control. Load control was estimated to be better than ± 1 pct. The effects of plate thickness, stress intensity (K) level and chemical environment on delay (or fatigue crack growth response), at room temperature, following a single high-load excursion or overload (see inset in Figure 1) were examined. The investigation was limited to an overload ratio (K_{1max}/K_{2max}) of 2.0, with the intervening fatigue loading at a load ratio (R) of 0.05.

Two different procedures were used to accommodate a number of overload tests on each specimen. In the first procedure, an attempt was made to achieve the same K_{1max} and K_{2max} at each overload point, and shall be designated hereafter as the "constant K" test. In the second procedure, the magnitudes of the loads were maintained constant; that is, "constant-load" test. In the constant K tests, the fatigue load magnitudes were selected to attain a desired value of K_{2max} at a pre-selected crack length. Fatigue loading was then interrupted, and a single overload cycle was applied, using the single cycle feature of the testing machine, with a triangular waveform at 0.01 Hz. Following the overload, fatigue loading was resumed at the same loading conditions immediately before the overload application and was continued to extend the crack beyond the point where steady-state rates were re-established (that is, beyond Point E in Figure 1). At this point, the fatigue loads were reduced such that the desired K_{2max} would be achieved at the next overload point. The change in K level within any overload-affected-zone was estimated to be less than

10 pct. The procedure was repeated until the desired number of overload tests were accomplished, and provided a number of tests at the same K_{2max} level. In the constant load test, the fatigue load magnitude was kept the same for each specimen. Overloads were applied in the same manner as that for the constant K tests. With this procedure, a number of K_{2max} values were examined using a single specimen.

Both of the procedures were used, in conjunction with a dc crack monitoring system, in studies on the 7.6 cm (3.0 in.) thick plate, and involved manual interruption and reinitiation for each of the overload tests. Fatigue cracking between overload was carried out under sinusoidally varying loads at 10 Hz. For the 1.65 cm (0.65 in.) thick plate, only the constant K procedure was used. Crack growth was measured by an ac crack monitoring system. The tests were fully automated and were controlled by an interactive digital computer. Fatigue cracking between overloads was carried out under sinusoidally varying loads at 20 Hz, and the overloads were applied using a triangular waveform at 0.01 Hz.

Crack Monitoring System

Both a dc and an ac electrical potential system were used for monitoring crack growth [29-32]. The dc system was used with specimens from the 7.6 cm (3.0 in.) thick plate, and the ac system was used for specimens from the 1.65 cm (0.65 in.) thick plate.

For the specimen geometry, analytical relationships between crack length and electrical potential were not available, and experimental calibration curves had to be established. Experimental calibrations were accomplished either by making simultaneous

visual and electrical potential measurements of crack length on specimens fatigued in air, or by comparing electrical potential measurements against fatigue markings on fracture surfaces produced by intentionally introduced high-load excursions (overloads) during fatigue in air. Calibration results are given in Figures 3 and 4.

The results in Figure 3a are dc measurements for the specimen configuration shown in Figure 2a at three specimen thicknesses, and are given as crack length (a) versus normalized potential (V^*).† These results show the reproducibility between specimens and confirm that the calibration curve is independent of specimen thickness. The following second degree polynomial, Eq. 2, provided the best (least-square) fit to the data, and was used as the calibration curve:

$$a = 0.792 + 3.43V^* - 1.54V^{*2} \quad (a \text{ in in.})$$
$$a = 2.01 + 8.71V^* - 3.91V^{*2} \quad (a \text{ in cm}) \qquad (2)$$

where a = crack length, $V^* = (V-V_r)/V_r$, V_r = reference potential associated with the initial notch, and V = V(a) = potential at a

†The electrical potential method provides measurements of crack length averaged through the thickness, while the visual method gives measurements of the crack length at the specimen surface only. Crack length measurements made by these two methods would differ because of crack front curvature. The discrepancy was significant for the thicker specimen. Corrections for crack front curvature were made by measuring average crack lengths from the fatigue markings (introduced during the calibration tests by changing the load amplitude) after specimen fracture. The average crack length was computed on the basis of five measurements - one at each specimen surface, one along each of the quarter-thickness planes and one along the mid-thickness plane. The "corrected" crack lengths are used in Figures 3 and 4 and in deriving Eqs. 2, 3 and 4.

crack length a. The calibration result in Figure 3b is for the specimen configuration shown in Figure 2b, at 1.65 cm (0.65 in.) thickness, using the dc measurement system. The corresponding calibration curve is given by Eq. (3).

$$a = 0.77 + 2.61V^{*2} - 0.26V^{*2} - 0.81V^{*3} \quad (a \text{ in in.})$$
$$a = 1.96 + 6.63V^{*} - 0.66V^{*2} - 2.06V^{*3} \quad (a \text{ in cm}) \qquad (3)$$

Accuracy of crack length measurement was estimated to be better than 1 pct for crack lengths from about 2 to 4.8 cm (0.8 to 1.85 in.). The resolution, based on a fixed working dc current of about 10 amperes, however, depended on specimen thickness, and was only slightly dependent on crack length. For the 1.27 cm (0.5 in.) thick specimen, crack length resolution was better than 0.005 cm (0.002 in.) based on 0.1μV resolution in electrical potential. Resolution for the other specimens varied in inverse proportion to the specimen thickness, that is, 0.007 cm, 0.002 cm and 0.001 cm (0.003 in., 0.0008 in. and 0.0004 in.) for the 1.65, 0.51, and 0.25 cm (0.65, 0.2, and 0.1 in.) thick specimens respectively.

Calibration results obtained from ac measurements on 1.65 cm (0.65 in.) thick specimens, with geometry shown in Figure 2b, are given in Figure 4 as crack length (a) versus potential difference $(V-V_r)$. The calibration results can be represented by Eq. (4).

$$a = 0.77 + 0.1586(V - V_r) \quad (a \text{ in in.})$$
$$a = 1.96 + 0.4028(V - V_r) \quad (a \text{ in cm}) \qquad (4)$$

V and V_r are defined in the same manner as that of the dc system and are given in microvolts. Because of variations in the

inductive contribution to V and V_r from specimen to specimen, normalization of electrical potential could not be used in this case. Unlike Eqs. (2) and (3), therefore, Eq. (4) is restricted to the particular specimen and operating current. Accuracy of crack length measurement with the ac system was estimated to be better than 1 pct also, for crack lengths from about 2 to 4.8 cm (0.8 to 1.85 in.). The resolution was better than 0.005 cm (0.002 in.) based on 12.5 nV resolution in electrical potential. Because of the use of a "lock-in" amplifier, better signal-to-noise ratio was obtained with the ac system.

Test Environment

The load interaction experiments were carried out in dehumidified argon, air and 3.5 pct sodium chloride solution (3.5 pct NaCl) at room temperature. For tests in dehumidified argon, the environment was maintained around the crack by flowing argon (purified by a suitable purification system) through chambers clamped to the faces of the specimen [31]. Tests in air were carried out with no special control (with relative humidity in the range of 30 to 70 pct). 3.5 pct NaCl solution was obtained by dissolving NaCl in triply distilled water. During testing, the solution was maintained around the crack in (inert) chambers attached to the specimen.

EXPERIMENTAL RESULTS

Fatigue crack growth response following a single high-load excursion (overload) is illustrated schematically in Figure 1. The actual experimental data (electrical potential versus time)

generally conformed to that depicted in Figure 1a, although the records invariably exhibited perturbations during and immediately following overload applications*. Fatigue crack growth response data are reported as the rate of crack growth (da/dN) versus relative crack position ($\Delta a_{OL} = a - a_{OL}$) with respect to the point of overload application (that is, in a form similar to Figure 1b), and correspondingly as da/dN versus ΔN_{OL} ($\Delta N_{OL} = N - N_{OL}$). The subscripts "OL" denote crack length and number of cycles at which an overload was applied.

To facilitate discussion, a number of formally defined plastic zone dimensions were computed and indicated on the appropriate figures. The dimensions include [33-35]:

Monotonic Overload Plastic Zone Size:

$$r_{p1} = \frac{1}{\pi}\left(\frac{K_{1max}}{\sigma_{ys}}\right)^2 \qquad \text{for plane-stress} \qquad (5)$$

$$r_{Ip1} = \frac{1}{3\pi}\left(\frac{K_{1max}}{\sigma_{ys}}\right)^2 \qquad \text{for plane-strain} \qquad (6)$$

Monotonic Plastic Zone Size Associated With Fatigue:

$$r_{p2} = \frac{1}{\pi}\left(\frac{K_{2max}}{\sigma_{ys}}\right)^2 \qquad \text{for plane-stress} \qquad (7)$$

$$r_{Ip2} = \frac{1}{3\pi}\left(\frac{K_{2max}}{\sigma_{ys}}\right)^2 \qquad \text{for plane-strain} \qquad (8)$$

*These perturbations introduced uncertainties into crack growth and growth rate measurements immediately following the overloads. These uncertainties are discussed in the Discussion section.

Cyclic Plastic Zone Size:

$$r_{pc} = \frac{1}{\pi}\left(\frac{\Delta K_2}{2\sigma_{ys}}\right)^2 \qquad \text{for plane-stress} \qquad (9)$$

$$r_{Ipc} = \frac{2}{3\pi}\left(\frac{\Delta K_2}{2\sigma_{ys}}\right)^2 \qquad \text{for plane-strain} \qquad (10)$$

σ_{ys} in Eqs. (5) to (10) is the yield strength in tension, and the zone sizes are equal to twice the formally calculated plastic zone correction factors (for example, $r_{p1} = 2\ r_{y1}$) [33-35].

For convenience, the results for specimens from the 7.6 cm (3.0 in.) thick and the 1.65 cm (0.65 in.) thick plates are reported separately. Note that experimental work on the 7.6 cm thick plate involved the use of a dc crack monitoring system, and required manual interruptions of the testing machine for overload applications. Tests on the 1.65 cm (0.65 in.) thick plate on the other hand were fully automated, and utilized an ac crack measurement system.

7.6 cm (3.0 in.) Thick Plate

Fatigue crack growth responses associated with a single high-load excursion (overload), with an overload ratio (K_{1max}/K_{2max}) of 2.0, for specimens of different thicknesses machined from the 7.6 cm thick plate and tested in different environments are shown in Figures 5 through 10. A number of overload experiments were carried out on each specimen. Individual runs on each specimen are designated sequentially by letters (A to E) or by numbers (1 to 5), and corresponded to increasing crack lengths at which the overloads were applied (a_{OL}). Fatigue cracking between

overloads were carried out under sinusoidally varying loads at a load ratio of 0.05, and frequency of 10 Hz.

Data from 0.25 cm (0.1 in.) and 1.27 cm (0.5 in.) thick specimens, tested in dehumidified argon using the "constant K" procedure at K_{2max} = 11 MN-m$^{-3/2}$ (10 ksi-in.$^{1/2}$), are shown in Figures 5 and 6. Two specimens were tested at each specimen thickness. There was considerable scatter in the data, but the overall trends were consistent, and did not suggest any significant influence of a_{OL} (that is, from proximity of the crack tip to the back edge of the specimen). Two of the specimens (F7-33-1 and CO-24-5) exhibited significant crack acceleration, while the other two did not. The growth rates decreased following the overload (and crack acceleration), and appeared to reach a minimum value after growing a distance equal to about r_{Ip2} or r_{p2} from the overload point. Thereafter, the rates increased until they re-established their equilibrium value. The overload affected zone appeared to be equal to about 1 r_{pl} for the thinner specimens, and to about 2 r_{Ipl} for the thicker specimen (Figure 5). Overall delay appeared to be longer for the thinner specimen than the thicker specimen (Figure 6) and is consistent with previous results on a 7075-T6 aluminum alloy [25]. These and other aspects of delay are discussed in a later section.

Comparable data from 0.51 cm (0.2 in.) and 1.27 cm (0.5 in.) thick specimens, tested in dehumidified argon using the "constant load" procedure, are shown in Figures 7 and 8. These results are consistent with those shown in Figures 5 and 6 with respect to the effects of specimen thickness on the sizes of delayed retardation

region and overload affected zone, and on delay. Both of the zone sizes increased with increasing K_{2max}.

Overload affected fatigue crack growth response data for a 0.51 cm (0.2 in.) thick specimen, tested in air by the "constant load" procedure, are shown in Figure 9. Comparison of Figures 7a and 9a shows that the rate of crack growth (both inside and away from the overload affected region) was faster in air than in dehumidified argon. The size of the overload affected zone, however, does not appear to be affected by the environment and is equal to about 1 r_{pl}. The size of the delay retardation region, on the other hand, appears to be much smaller for the specimen tested in air (being approximately equal to the cyclic plastic zone size r_{Ipc}), and delay appears to be shorter in air (compare Figures 7a, 8a and 9). The dependence of these zone sizes on K level are reflected through their dependence on the plastic zone sizes (r_{pl} and r_{Ipc}).

The effects of environment on fatigue crack growth response in this material are more readily seen in Figure 10. Data from 0.51 cm (0.2 in.) thick specimens tested in dehumidified argon and in air, and for 0.76 cm (0.3 in.) thick specimen tested in 3.5 pct NaCl solution are compared at $K_{2max} \approx 10.8$ MN-m$^{-3/2}$ (9.8 ksi-in.$^{1/2}$). The results again suggest that the overload affected zone was essentially independent of environment. The rates of crack growth, on the other hand, were affected by the test environment, thereby reducing delay for the more aggressive environments.

1.65 cm (0.65 in.) Thick Plate

To further examine the influences of environment and K level

on fatigue crack growth response associated with a single high-load excursion (overload), experiments were carried out in dehumidified argon, air and 3.5 pct NaCl solution on the 1.65 cm thick plate. Two stress intensity levels (K_{2max} = 8.8 and 15.4 MN-m$^{-3/2}$ or 8.0 and 14.0 ksi-in.$^{1/2}$), with an overload ratio (K_{1max}/K_{2max}) of 2.0, were used. Fatigue crack growth was carried out under sinusoidal loading at a stress ratio of 0.05 and a frequency of 20 Hz. The "constant K" procedure was utilized, and the entire experiment was fully automated. Six over-load tests were run on each specimen. Data associated with each over-load test are designated by a number from 1 to 6; the numbers correspond to increasing a_{OL}.

Experimental data for tests in dehumidified argon are shown in Figure 11; those for tests in air, in Figures 12 and 13; and those for tests in 3.5 pct NaCl solution in Figures 14 and 15. Because of more precise control afforded by the automated testing procedure, there was considerably less scatter in these results as compared with those on the 7.6 cm (3.0 in.) thick plate material (see Figures 5 to 8 for example). The results show that the overload affected zone extended out a distance of about 2 r_{Ip1} from the point of overload application and was essentially independent of the test environment. The data also indicate that the delayed retardation region was considerably smaller than the monotonic plastic zone size (r_{Ip2}) and was of the order of the cyclic plastic zone size (r_{Ipc}). Delay in the aggressive environments (air and 3.5 pct NaCl solution) was shorter than in dehumidified argon, although there was no discernible difference between delay (or the rate of crack growth) in air and in 3.5 pct NaCl solution for the two

K_{2max} levels at 20 Hz. Longer delay was observed at the lower K_{2max} level in both environments (Figures 13 and 15). The observed trend on delay is in agreement with previous results on Ti-6Al-4V alloy [21-24].

DISCUSSION

Data Scatter

Considerable amounts of scatter were observed in the data for specimens taken from the 7.6 cm (3.0 in.) thick plate, particularly for those obtained under "constant K" conditions (see Figures 5 and 6, for example). Several sources contributed to this scatter; all of which are difficult to quantify but are interrelated. First, the dc electrical potential system for monitoring crack growth readily responds to external disturbances, such as interruptions in load and changes in temperature, and has lower noise rejection capabilities than the ac system. Interruptions in testing to apply overloads tended to perturb the system, which required some time (order of minutes) to re-establish equilibrium. During these periods of perturbation, the potential measurements can be in error by several tenths of microvolts (corresponding to errors in crack lengths of say 0.015 cm or 0.006 in. for 0.3μV disturbance in the 1.27 cm thick specimens, and lesser amounts in the thinner samples). Errors in crack growth rates may reach the order of ± 50 pct. Second, the testing procedure itself can be sources for scatter. The manual interruption procedure used in conjunction with overload application and the resumption of fatigue required "manual" setting and adjustment of loads.

Each load change required time, which cannot always be controlled. The variations in these "setup" times contributed to scatter in two ways: (a) It altered the period of perturbation for the crack monitoring system, and thereby contributed to scatter as discussed previously; and (b) the time at minimum load (and possibly under slight compressive load) could alter the subsequent crack growth response [21,22]. Other sources of variability included accuracy in estimating K during testing (specifically for computing K_{2max} and K_{1max} at the overload points), nonconstancy of K, the influence of crack length on the rate of change of K with crack growth, etc. Overall, uncertainty in Δa_{OL} and da/dN, immediately following the overload, can vary by the amounts estimated previously.

Because of the use of automated control and of the improved ability for rejecting external disturbances with the ac potential system, scatter in data from the 1.65 cm (0.65 in.) thick plate was much smaller. Uncertainty in Δa_{OL} was estimated to be better than 0.005 cm (0.002 in.) for the 1.65 cm (0.65 in.) thick specimens. Uncertainty in crack growth rates was estimated to be about ± 20 pct. Greater reliance, therefore, will be placed on the data from the 1.65 cm thick plate in the interpretation of experimental results.

In addition to these sources of scatter, the proximity of the back edge of the specimen at long crack lengths (greater than, say, 4 cm) may have also affected the test results. This possible effect is suggested by data on the 1.65 cm thick specimens (see data set labeled as "6" in Figures 11 to 15). Such an influence,

however, was not apparent in the data on specimens machined from the 7.6 cm thick plate (see Figures 5 and 6); although the effect might have been obscured by scatter introduced from other sources. Further tests would be needed to better establish the existence and significance of this effect.

Overload Affected Zone and Delayed Retardation Zone

In spite of the scatter in some of the data, a reasonably consistent trend is evident in all of the data, and conforms to that illustrated schematically in Figure 1. The high-load excursion (overload) affected a zone of material ahead of the crack tip. This overload affected zone is delineated by the point of overload application to the point where steady-state fatigue crack growth is re-established (that is, the distance from Point B to Point E in Figure 1b). Within the overload affected zone, fatigue crack growth response included (a) an abrupt increase in growth rate to a value greater than the steady-state rate (or crack acceleration), (b) a fairly rapid decrease in rate to a minimum value (delayed retardation) over some small distance ahead of the crack-tip (delayed retardation zone), and (c) subsequent gradual increase in rate back to the steady-state value.

Examination of Figures 5, 7, 9a, 10a, 11a, 12 and 14 suggests that, for the 2219-T851 aluminum alloy, the overload affected zone is essentially equal to the monotonic plastic zone size associated with the overload K, that is K_{1max}, see Eqs. (5) and (6) [8,10,11]*.

*Because of the contribution of surface shear lips to delay [22, 25], the lower bound for Z_{OL} may be larger than r_{Ipl}, and appears to be equal to about 2 r_{Ipl} for this 2219-T851 aluminum alloy over the range of specimen thickness and K_{1max} values used in this investigation.

Depending on specimen thickness and K_{1max}, the appropriate zone size may range between that for "plane-strain" (r_{Ipl}) and that for "plane-stress" (r_{pl}). The zone sizes are indicated on the various figures. The overload affected zone size thus obviously depends on K_{1max} and on specimen thickness, but does not appear to be dependent on the test environment (see Figure 10 and compare Figures 11a, 12 and 14). Since the overload affected zone resulted principally from mechanical interactions, the apparent independence of zone size on test environment is reasonable.

Significant crack acceleration was observed in some cases and not in others, and was more prevalent for tests in dehumidified argon (an inert environment) than in air and in 3.5 pct NaCl solution (aggressive environments), see Figures 5 and 15. No systematic behavior was obvious, and the crack acceleration phenomenon would require further examination.

Delayed retardation appeared to take place over an increment of crack growth (Δa_{OL}) that ranged from the cyclic plastic zone size, Eqs. (9) and (10), to the monotonic plastic zone size, Eqs. (7) and (8), associated with the fatigue loading (that is, ΔK_2 or K_{2max}). Depending on the stress intensity level and specimen thickness, again, the appropriate zone size may be either that for "plane-strain" or that for "plane-stress". In light of the smaller amount of scatter in data on the 1.65 cm thick plate, one might suggest that the delayed retardation zone size be considered to be equal to the cyclic plastic zone size. The existence of delayed retardation then may be interpreted in terms of the growth of the crack through a region that had already experienced cyclic fatigue damage.

Effects of Specimen Thickness, Environment and K Level on Delay

Having established that the overload affected zone depended on specimen thickness and K level (that is, on crack-tip constraint) and was essentially independent of test environment, the influences of these variables on delay (or N_D^*) may now be considered. Delay in essence represents the number of fatigue load cycle that is required to extend the crack through the overload affected zone. As such, it is proportional to the zone size and is inversely proportional to the average rate of crack growth through the overload affected zone.

For specimens of different thicknesses, the overload affected zone sizes are different, with larger zone sizes associated with the thinner specimens (that is, those tending toward "plane-stress"). For the range of K levels used in investigation, the rate of fatigue crack growth in a given environment was sensibly independent of specimen thickness [36,37]. Hence, the thinner specimens would tend to experience greater delay (see Figures 6 and 8). This observation is consistent with results on other aluminum alloys [25,26].

A similar argument can be applied in considering the effects of environment. Since the overload affected zone size does not alter with environment, delay (N_D^*) would simply vary inversely with the fatigue crack growth rate. Delay in the more aggressive environment, therefore, would be expected to be shorter, which is consistent with observations (see Figures 10b, 11b, 13 and 15)*.

*Note that in Figures 13 and 15, there was little difference in the rate of fatigue crack growth and in delay between tests in air and in 3.5 pct NaCl at a loading frequency of 20 Hz.

Interpretation of the effects of K level is less straightforward because increasing K increases both the overload affected zone size and the rate of fatigue crack growth. The net effect, however, resulted in a decrease in delay in this material (see Figures 9b, 13 and 15). This observation is consistent with previous results on a Ti-6Al-4V alloy [21-24], but differed with some results on a 7075-T6 aluminum alloy [25]. The difference presumably may be attributed to the use of N_D instead of N_D^* in the previous experiments [25] (see Figure 1). Data from this investigation suggest that N_D may be less than one-half of N_D^* when there is significant crack acceleration following an overload.

Modeling Considerations

A number of models have been suggested to account for the effects of high-load excursions (overloads) on the subsequent fatigue crack growth response [7-15]. A suitable model, however, should include a description of crack acceleration and delayed retardation, as well as one for the recovery to steady-state crack growth rate. Since the modified Willenborg et al. model [10-12] appeared to provide useful results, a comparison of this model with the present results seemed appropriate. Specifically, this comparison pertained to its ability to predict the recovery stage of crack growth since the model does not account for crack acceleration and delayed retardation. Because both constant-amplitude fatigue crack growth and delay data are available for dehumidified argon, a comparison for this environment was made. Specifically, data obtained on a 1.65 cm thick specimen at K_{2max} = 15.4 MN-m$^{-3/2}$ (14 ksi-in.$^{1/2}$), Figure 11, were used, and comparison with model predictions is shown in Figure 16.

According to the modified Willenborg et al. model [10-12], the stress intensity factors for fatigue are to be reduced by a residual stress intensity factor K_R that decayed linearly with crack extension. In terms of notations used here, K_R is given as follows:

$$K_R = \Phi\ K_R^W = \frac{(1 - K_{th}/K_{2max})}{S - 1} \left[K_{1max} \left(1 - \frac{\Delta a_{OL}}{Z_{OL}} \right) - K_{2max} \right] \quad (11)$$

K_{th} is the maximum stress intensity factor associated with fatigue crack growth threshold at R = 0; Δa_{OL} is crack growth following the overload; and Z_{OL} is the overload affected zone*. S is defined as a shut-off ratio, and corresponds to that value of the ratio of K_{1max}/K_{2max} where crack arrest is expected to result. Taking $Z_{OL} = 4r_{Ipl} = 0.312$ cm (0.124 in.) and an assumed value of K_{th} of 4.4 MN-m$^{-3/2}$ (4.0 ksi-in.$^{1/2}$) [12,36-39], values of K_R were computed for two shut-off ratios (that is, S = 2.3 and 2.8)**. These values of K_R were used to compute effective stress intensity factors at different values of Δa_{OL}, which were used in turn to determine the corresponding fatigue crack growth rates from constant-amplitude data [36-39]. The model predictions are shown as dashed lines in Figure 16.

Inspection of Figure 16 indicates that better agreement was obtained by using S = 2.8. The modified Willenborg et al. model,

---

* Z_{OL} was taken to be $(\gamma/2\pi)(K_{1max}/\sigma_{ys})^2$, where γ is an empirical constant [12].

**Shut off ratio of 2.3 corresponded to the value used by Gallagher and Stalnaker [12], and S = 2.8 corresponded to data on a Ti-6Al-4V alloy [21,22].

however, appeared to underestimate the rate of recovery to steady-state growth. This observation suggests that a faster decay in K_R would be required. Furthermore, because the model presumed that the effect of overload was exhausted when the "leading edge" of the fatigue-crack plastic zone reached the boundary of the overload plastic zone, an overload-affected-zone that was larger than the overload plastic zone (in this case, $Z_{OL} = 4r_{Ipl}$) had to be assumed to model the recovery response (see Figure 16). The results, on the other hand, suggested that the overload affected zone was equal to the overload plastic zone size ($\sim 2\, r_{Ipl}$). The exhaustion of overload effect would therefore correspond to the emergence of the fatigue crack from the overload plastic (or overload affected) zone, which provides certain physical appeal.

Based on these observations and on the experimental data, it appeared reasonable to suggest further semi-empirical modifications to the model of Willenborg et al. [8]. In these further modifications, the basic concept of a residual stress intensity factor K_R produced by the overload is preserved. The rate of decay of K_R is assumed to be proportional to $(1 - \Delta a_{OL}/Z_{OL})^2$ over a range of Δa_{OL} from Z^*_{OL} to Z_{OL}, viz.:

$$K_R = K^\circ_R \, (1 - \Delta a_{OL}/Z_{OL})^2; \; Z^*_{OL} \leq \Delta a_{OL} \leq Z_{OL} \qquad (12)$$

Z^*_{OL} is the delayed-retardation-zone size and is assumed to be equal to the appropriate cyclic plastic zone size (or plastic zone size). Z_{OL} is the overload-affected-zone size and is taken to be equal to the appropriate overload plastic zone size. K°_R is the residual stress intensity factor at $\Delta a_{OL} = 0$ (that is, immediately

following the overload) and is given by [8,12].

$$K_R^\circ = \frac{(1 - K_{th}/K_{2max})}{(S - 1)} (K_{1max} - K_{2max}) \quad (13)$$

or

$$K_R^\circ = (1 - K_{th}/K_{2max}) \frac{(Q - 1)}{(S - 1)} K_{2max} \quad (14)$$

$Q = K_{1max}/K_{2max} \geq 1$ is the overload ratio. Crack arrest is expected to occur when $Q \geq S$ [12].

According to this modified model, a minimum in crack growth rate following an overload would be expected to occur at $\Delta a_{OL} = Z^*_{OL}$ and assume a value corresponding to the effective stress intensity factor at that point, as determined from Eq. (12). Delayed retardation response may be, as a first order approximation, obtained by joining a straight line between the point of overload application and the minimum growth rate point (at $\Delta a_{OL} = Z^*_{OL} = r_{Ipc}$), and could be expressed in exponential form, if desired. Recovery in crack growth would be described in a manner similar to the original model by using K_R given by Eq. (12). Estimated response based on this modified model (neglecting crack acceleration) is indicated by the solid line in Figure 16 for S = 2.8, and is seen to be in good agreement with the data. Comparable agreement was obtained with data from the 7.6 cm thick plate (that is, data shown in Figures 5 and 6). Further development of this empirical model and experimental verification are needed.

SUMMARY

To expand on the phenomenological understanding of the

effects of load interactions on fatigue (principally delay), the influences of plate thickness, K level and chemical environment on fatigue crack growth response following a single high-load excursion (overload) were examined for a 2219-T851 aluminum alloy. An overload ratio (K_{1max}/K_{2max}) of 2.0 was used. The principal results of this investigation are as follows:

1. The high-load excursion (overload) affected a region of material ahead of the crack tip, within which fatigue crack growth deviated from its steady-state behavior. The size of the overload affected zone was dependent on the crack-tip constraint, and was thereby dependent on K level and specimen thickness. For a given K level and specimen thickness, the overload affected zone for the 2219-T851 alloy was independent of chemical environment and was found to be about equal to the appropriate (plane-strain or plane-stress) plastic zone size (diameter) for the high load (or K_{1max}) (viz., 2 r_{Ipl} for "plane-strain" and r_{pl} for plane-stress").

2. Delay (N_D^*) was found to increase with decreasing specimen thickness. This increase in delay may be attributed primarily to an enlargement in the overload-affected-zone size for the thinner specimens.

3. Delay (N_D^*) was found to decrease with increasing aggressiveness of the environment (that is, dehumidified argon → air → 3.5 pct NaCl solution). This decrease in delay may be attributed to the higher rates of fatigue crack growth in the more aggressive environments.

4. Decreasing K level produced an increase in delay in this alloy. This dependence on K was the net result of the separate

influences of K on the overload-affected-zone size and on the rate of fatigue crack growth.

5. The results provided further confirmation of delayed retardation, and suggested that this phenomenon is associated with crack growth through a region of material within the overload affected zone that had sustained prior fatigue damage. Based on this interpretation, it is suggested that a delayed retardation zone be defined, and that the size of this zone be identified with the cyclic plastic zone size associated with steady-state fatigue immediately preceding the overload. Minimum in the rate of fatigue crack growth within the overload affected zone may be expected to occur at the delayed retardation zone boundary. These suggestions tended to be supported by the data, although some of the data suggested that this zone size may be as large as the monotonic plastic zone diameter associated with prior fatigue.

6. A residual stress intensity factor (K_R) concept appeared to be useful in describing fatigue crack growth response following an overload application. A further modification to the model of Willenborg *et al.*, to increase the rate of decay in K_R, was suggested. This modification appeared to provide reasonable estimates of fatigue crack growth response.

ACKNOWLEDGEMENT

The authors express their sincere appreciation to Mr. C. D. Miller for his assistance with the experimental work, and to Mr. R. Brazill for his assistance in developing the computer program used in the automated test procedure. Support of this work by the

Air Force Office of Scientific Research under Grant AFOSR-75-2857 is gratefully acknowledged.

REFERENCES

1. Christensen, R. H., Proceedings - Crack Propagation Symposium, Cranfield, College of Aeronautics (1962).

2. Schijve, J., Fatigue Crack Propagation in Light Alloy Sheet Material and Structures, Rept. MP 195, National Luchtvaart-laboratorium (Amsterdam), (August 1960).

3. Hudson, C. M., and Hardrath, H. F., NASA TN D-960, (1961).

4. Hudson, C. M., and Raju, K. N., NASA TN D-5702, (1970).

5. Butler, J. P., "The Material Selection and Structural Development Process for Aircraft Structural Integrity Under Fatigue Conditions", AFFDL TR-70-144 (1970), 17, Air Force Flight Dynamics Lab., WPAFB, Ohio.

6. Fatigue Crack Growth Under Spectrum Loads, ASTM STP 595 (1976).

7. Wheeler, O. E., Trans. ASME, Ser. D, 94 (1972), 123.

8. Willenborg, J. D., Engle, R. M., Jr., and Wood, H. A., AFFDL-TM-71-1-FBR (January 1971), Air Force Flight Dynamics Lab., WPAFB, Ohio.

9. Elber, W., ASTM STP 486 (1971), 230.

10. Gallagher, J. P., and Hughes, T. F., "Influence of Yield Strength on Overload Affected Fatigue Crack Growth Behavior in 4340 Steel", AFFDL-TR-74-27 (July 1974), Air Force Flight Dynamics Lab., WPAFB, Ohio.

11. Petrak, G. J., and Gallagher, J. P., Trans. ASME, Ser. H, 97 (1975), 206-213.

12. Gallagher, J. P., and Stalnaker, H. D., J. Aircraft, 12 (1975), 699-705.

13. Schijve, J., ASTM STP 595 (1976), 3.

14. Bell, P. D., and Wolfman, A., ASTM STP 595 (1976), 157.

15. Jacoby, G. H., Nowack, H., and van Lipzig, H. T. M., ASTM STP 595 (1976), 172.

16. Dill, H. D., and Saff, C. R., ASTM STP 595 (1976), 306.

17. Wood, H. A., and Haglage, T. L., AFFDL-TM-71-2-FBR (January 1971), Air Force Flight Dynamics Lab., WPAFB, Ohio.

18. Wood, H. A., Haglage, T. L., and Engle, R. M., Jr., AFFDL-TM-71-3-FBR (1971), Air Force Flight Dynamics Lab., WPAFB, Ohio.

19. Matthews, W. T., Baratta, F. I., and Driscoll, G. W., Intl. J. Fract. Mech., 7 (1971), 224.

20. von Euw, E. F. J., Hertzberg, R. W., and Roberts, R., ASTM STP 513 (1972), 230.

21. Jonáš, O., and Wei, R. P., Int'l. J. Fract. Mech., 7 (1971), 116-118.

22. Wei, R. P., and Shih, T. T., Int'l. J. Fract., 10 (1974), 77.

23. Shih, T. T., and Wei, R. P., Prospects of Fracture Mechanics, Noordhoff (1974), 231.

24. Shih, T. T., and Wei, R. P., ASTM STP 595 (1976), 113.

25. Shih, T. T., and Wei, R. P., J. Testing and Evaluation, ASTM, 3 (1975), 46.

26. Mills, W. J., and Hertzberg, R. W., Eng. Fract. Mech., 7 (1975), 705.

27. Wilson, W. K., "Analytical Determination of Stress Intensity Factors for the Manjonie Brittle Fracture Test Specimen", Report No. WERL-0029-3, Westinghouse Research Laboratories (1965).

28. Wilson, W. K., "Optimization of WOL Brittle Fracture Test Specimen", Report No. 66-1B4-BTLFR-R1, Westinghouse Research Laboratories (1966).

29. Johnson, H. H., Mater. Res. and Std., 5 (1965), 442.

30. Li, C. Y., and Wei, R. P., Mater. Res. and Std., 6 (1966), 392.

31. Gangloff, R. P., and Wei, R. P., Met. Trans. A, 8A (1977), 1043.

32. Wei, R. P., unpublished results on ac potential system (1977).

33. Irwin, G. R., in Structural Mechanics, Pergamon Press (1960), 557.

34. McClintock, F. A., and Irwin, G. R., ASTM STP 381 (1965), 84.

35. Rice, J. R., ASTM STP 415 (1967), 247.

36. Unangst, K. D., Shih, T. T., and Wei, R. P., Eng. Fract. Mech., 9 (1977), 725.

37. Unangst, K. D., Shih, T. T., and Wei, R. P., "Crack Closure and Fatigue Crack Growth in 2219-T851 Aluminum Alloy", Interim Report, AFOSR-TR-76-1247 (August 1976)(ADA633082).

38. FitzGerald, J. F., J. Testing and Evaluation, ASTM, 5 (1977), 343.

39. Pao, P. S., and Wei, R. P., unpublished results (1978).

Table 1

Chemical Composition and Tensile Properties of 7.6 cm (3-in.) thick 2219-T851 Aluminum Alloy Plate*

a. Chemical Composition (Weight Percent)

Cu	Zn	Mg	Si	Mn	Ti	Cr	Fe	Al
6.28	0.025	0.003	0.088	0.25	0.051	<0.0001	0.25	Balance

b. Tensile Properties**

Orientation	Yield Strength MN/m^2 (ksi)	Tensile Strength MN/m^2 (ksi)	Elongation in 5.08 cm pct	Reduction of Area pct
Longitudinal	358 (52)	455 (66)	8.5	19
Transverse	351 (51)	455 (66)	8.2	19

* Data from Westinghouse Electric Corporation.
** Averages of 6 tests from 2 locations.

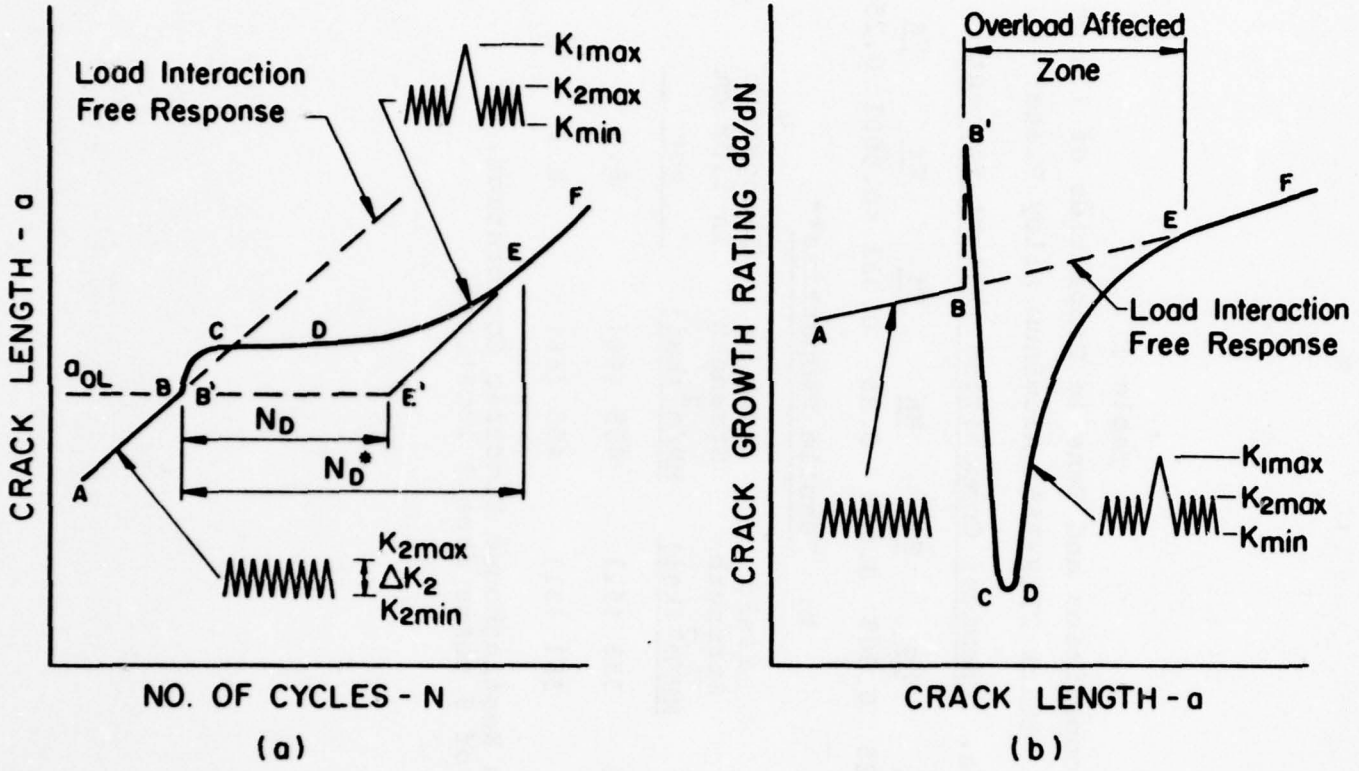

Figure 1: Schematic illustration of fatigue crack growth response following a single high-load excursion (overload), and definition of N_D and N_D^*.

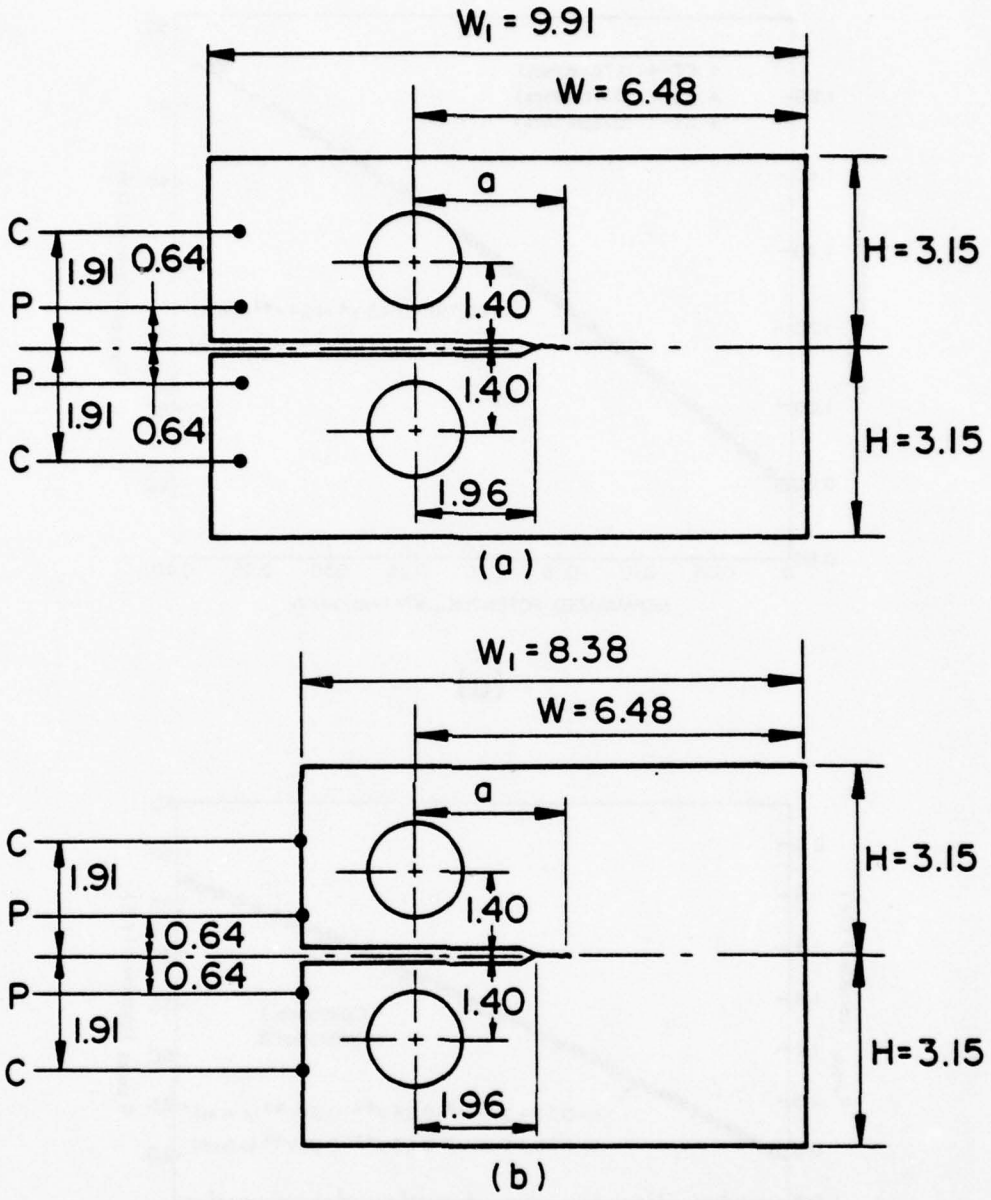

Notes: All dimensions in cm (2.54 cm = 1 in.)
C = current leads; P = potential leads

Figure 2: Wedge-opening-load (WOL) specimens and placement of current and potential leads for the crack monitoring system.

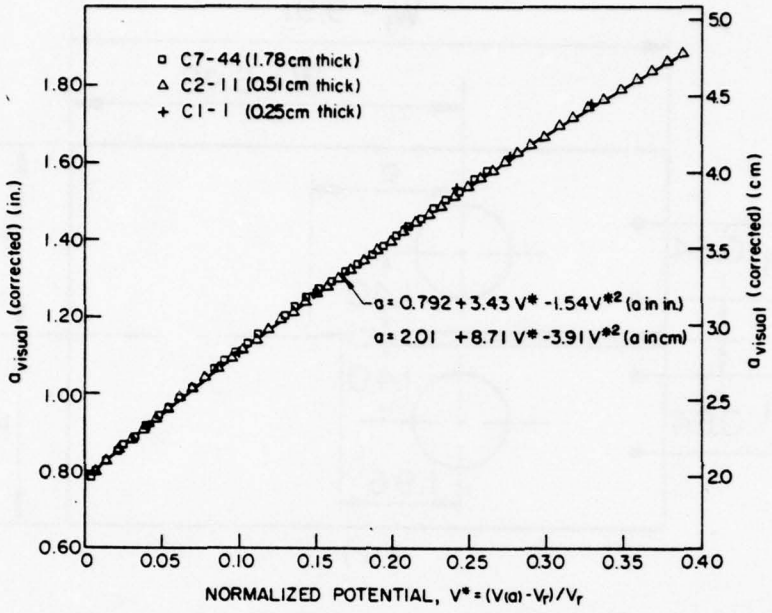

(a)

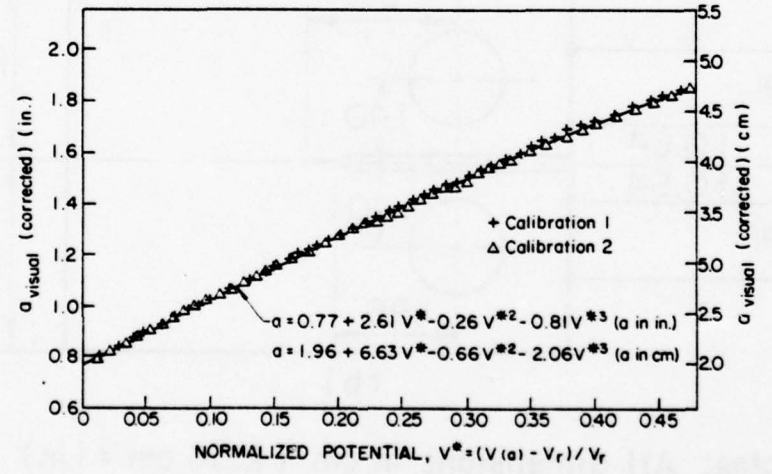

(b)

Figure 3: Calibration curve for crack length versus normalized dc potential for specimens from (a) the 7.6 cm thick plate (see Figure 2a), and (b) the 1.65 cm thick plate (see Figure 2b).

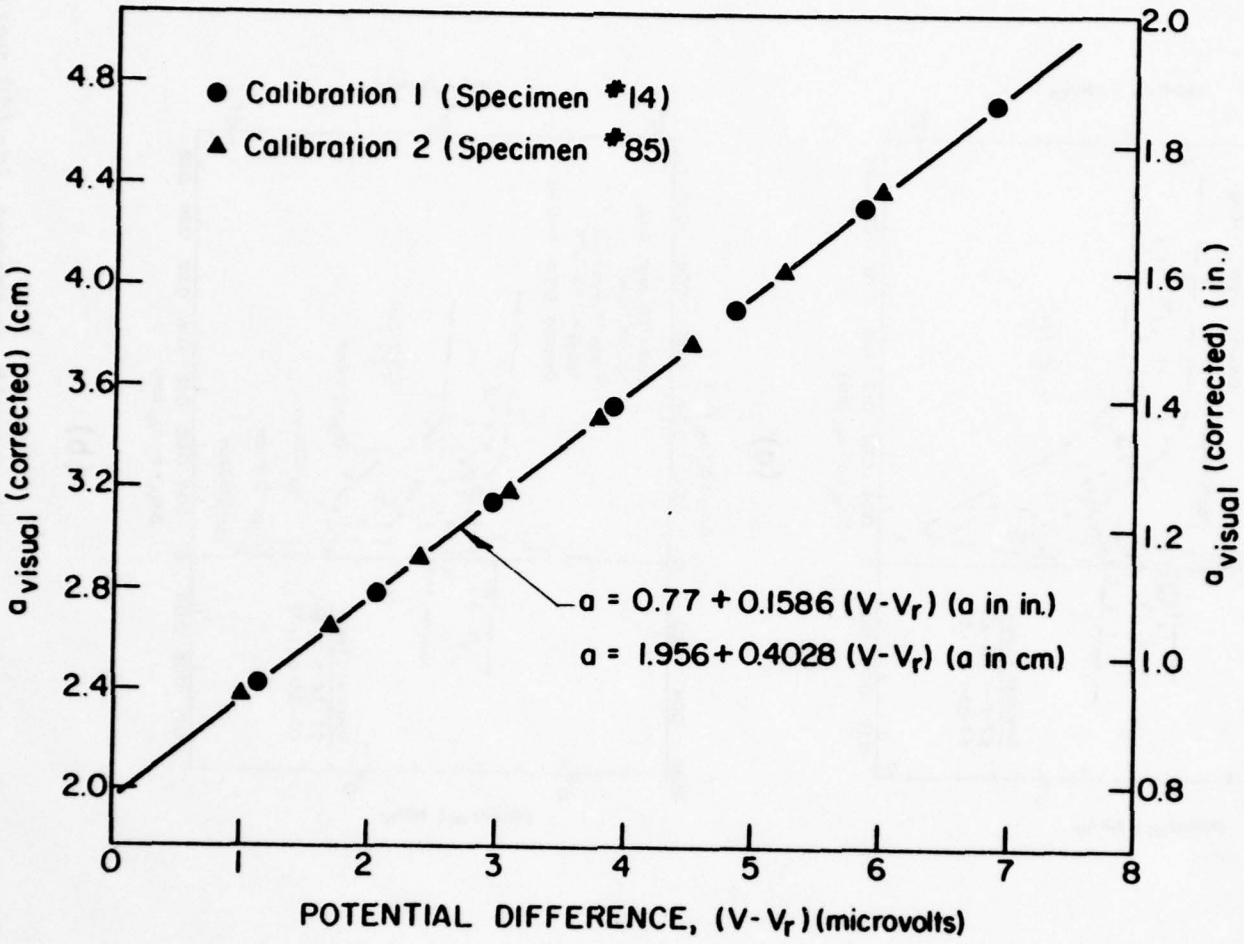

Figure 4: Calibration curve for crack length versus change in ac potential for specimens from the 1.65 cm (0.65 in.) thick plate. (See Figure 2b.)

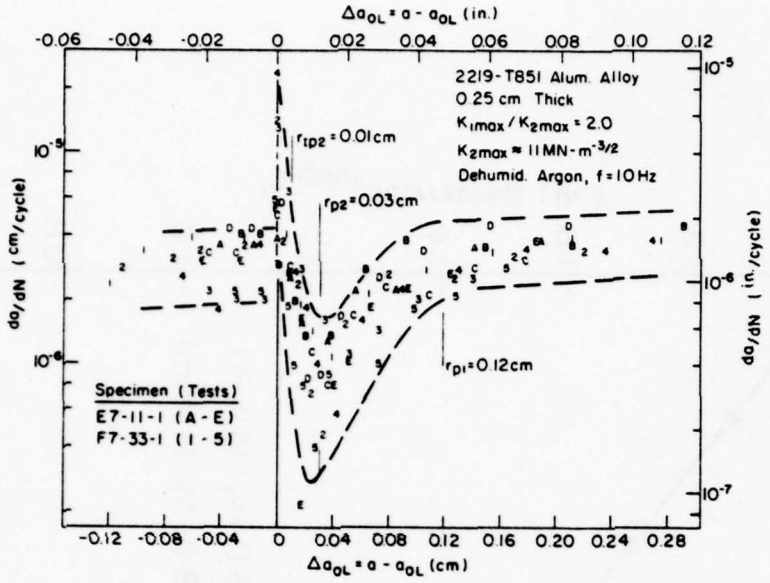

(a)

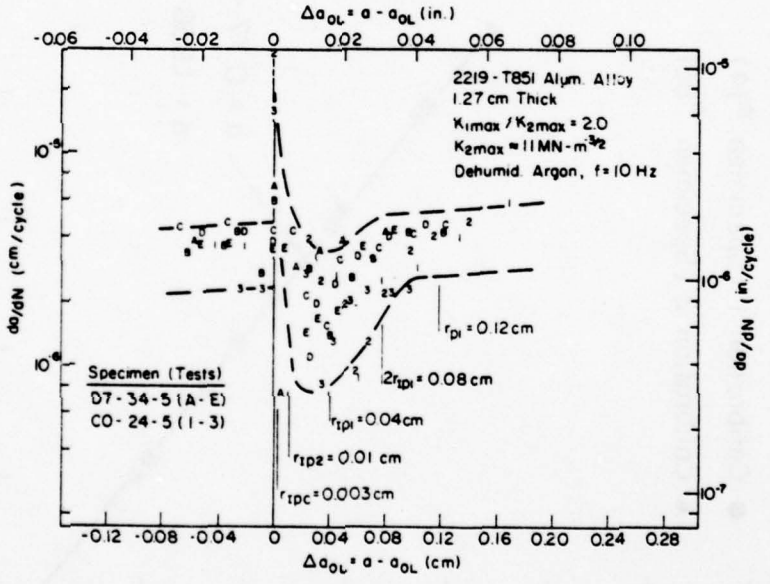

(b)

Figure 5: Fatigue crack growth response (da/dN versus Δa_{OL} following a single overload at $K_{1max}/K_{2max} = 2.0$ using the "constant K" procedure: (a) 0.25 cm thick specimens, and (b) 1.27 cm thick specimens. (Test environment: dehumidified argon at room temperature. Fatigue loading at R = 0.05).

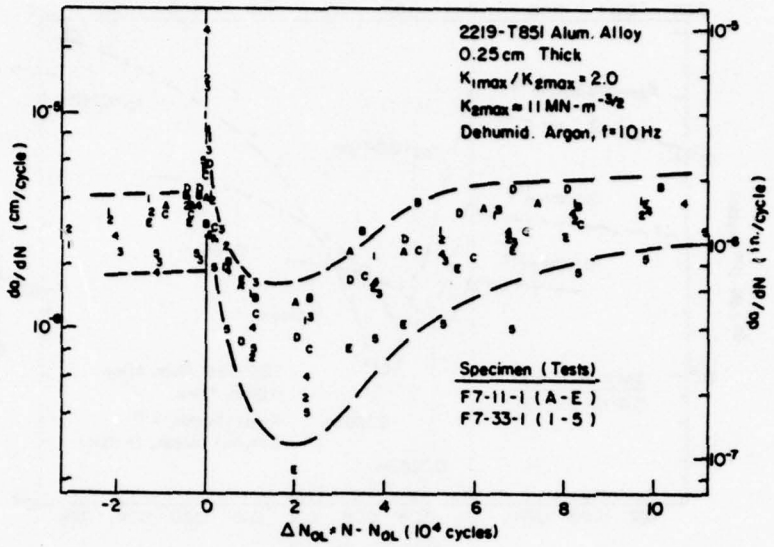

(a)

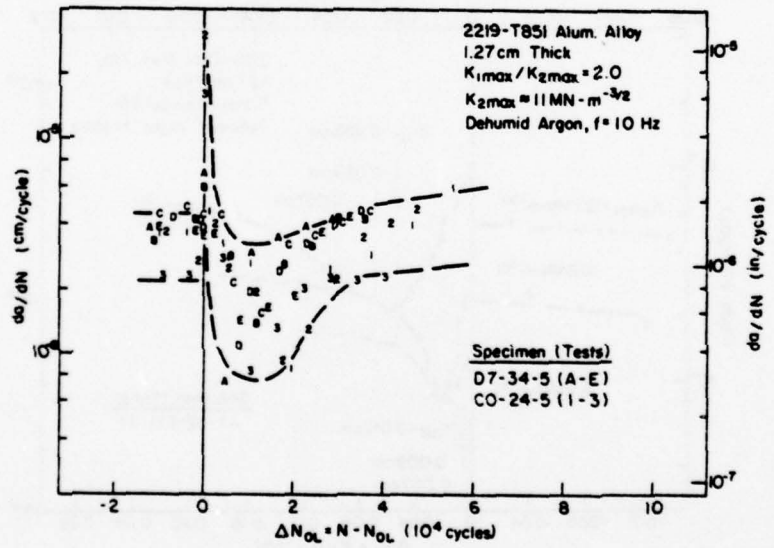

(b)

Figure 6: Fatigue crack growth response (da/dN versus ΔN_{OL}) following a single overload at $K_{1max}/K_{2max} = 2.0$ using the "constant K" procedure: (a) 0.25 cm thick specimens, and (b) 1.27 cm thick specimens. (Test environment: dehumidified argon at room temperature. Fatigue loading at R = 0.05).

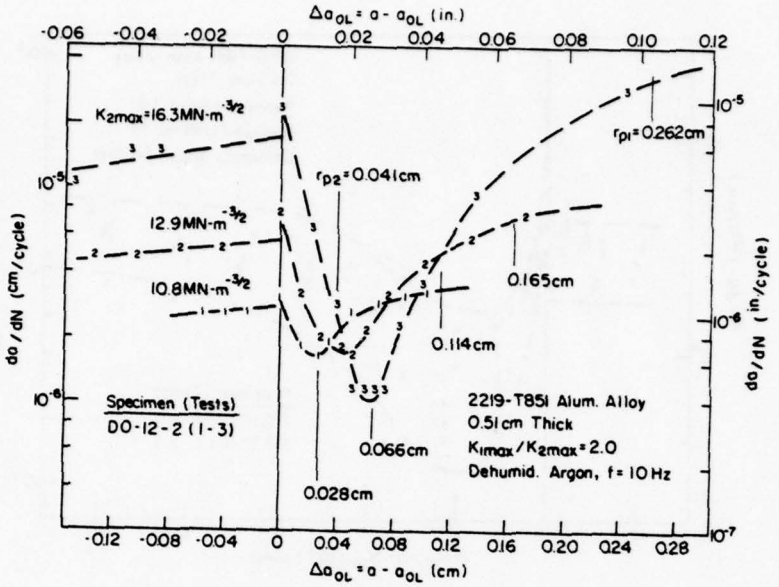

(a)

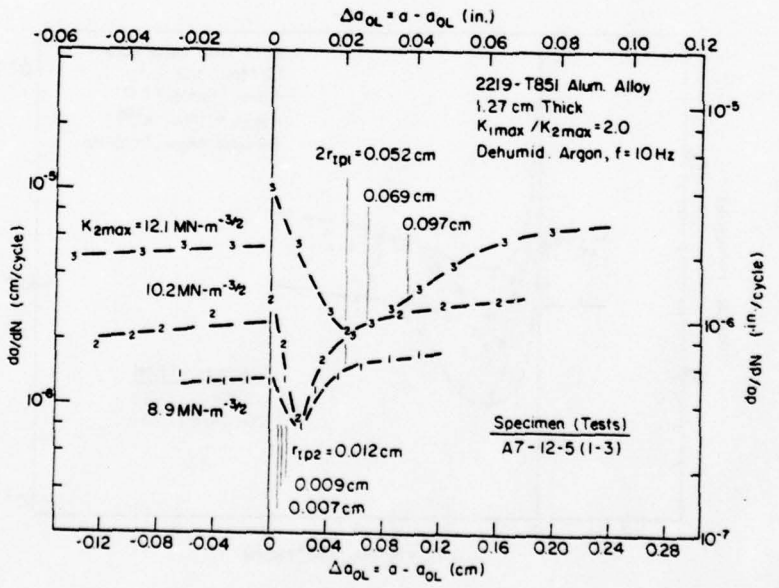

(b)

Figure 7: Fatigue crack growth response (da/dN versus Δa_{OL}) following a single overload at K_{1max}/K_{2max} = 2.0 using the "constant load" procedure; (a) 0.51 cm thick specimen, and (b) 1.27 cm thick specimen. (Test environment: dehumidified argon at room temperature. Fatigue loading at R = 0.05).

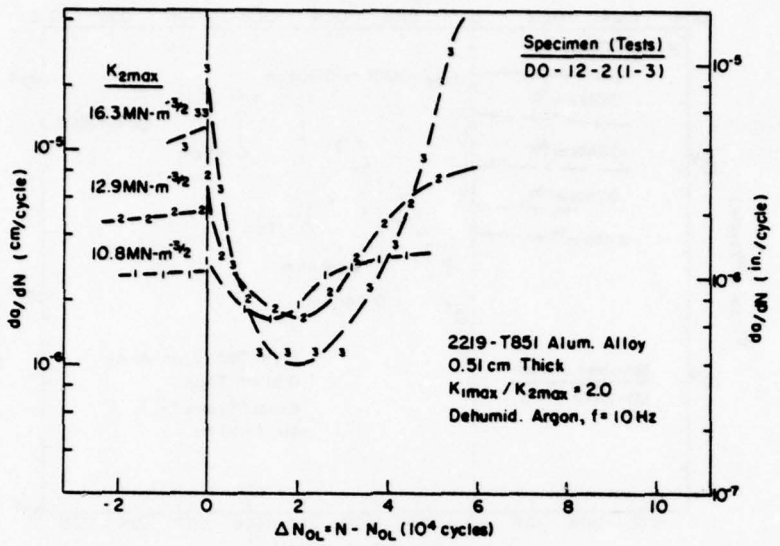

(a)

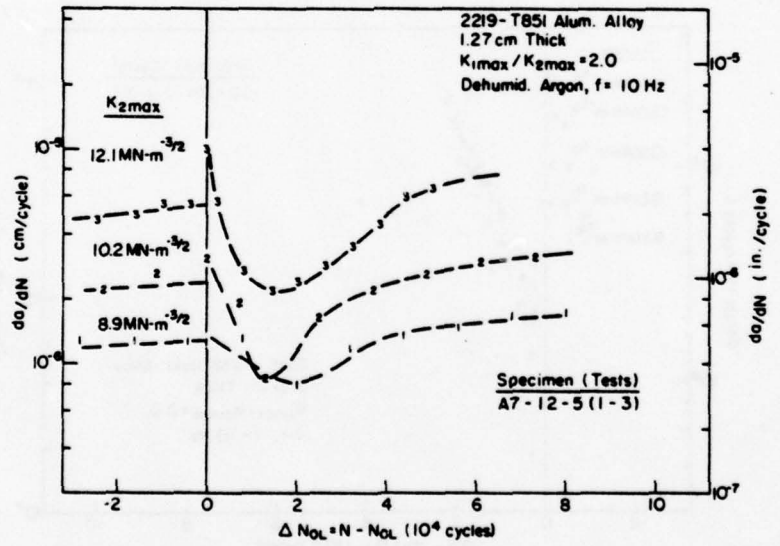

(b)

Figure 8: Fatigue crack growth response (da/dN versus ΔN_{OL}) following a single overload at K_{1max}/K_{2max} = 2.0 using the "constant load" procedure: (a) 0.51 cm thick specimen, and (b) 1.27 cm thick specimen. (Test environment: dehumidified argon at room temperature. Fatigue loading at R = 0.05).

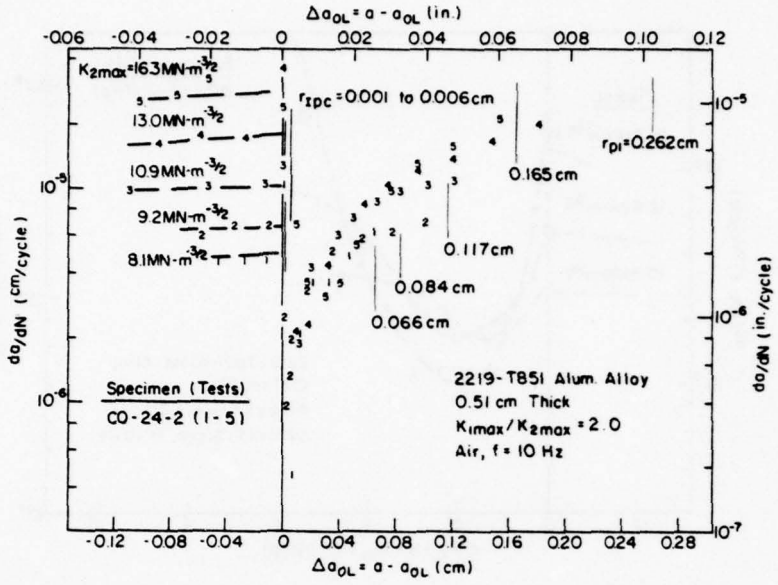

(a)

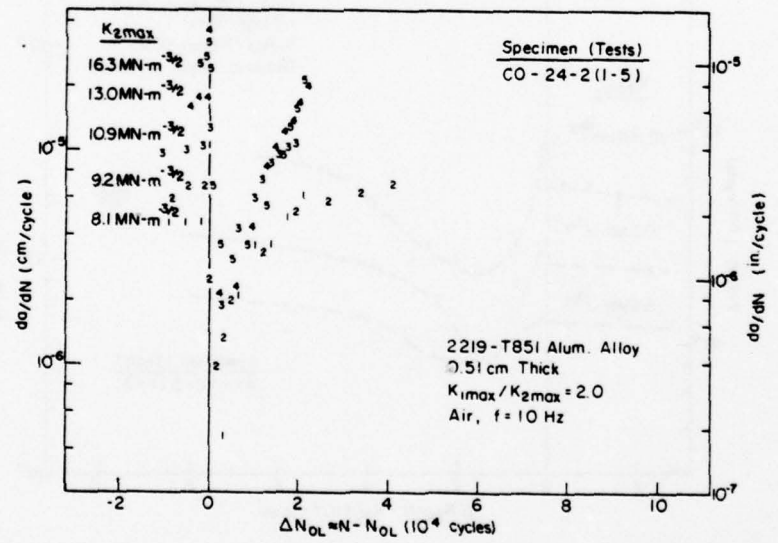

(b)

Figure 9: Fatigue crack growth response for a 0.51 cm thick specimen following a single overload at K_{1max}/K_{2max} = 2.0 using the "constant load" procedure: (a) da/dN versus Δa_{OL}, and (b) da/dN versus ΔN_{OL}. (Test environment: air at room temperature. Fatigue loading at R = 0.05).

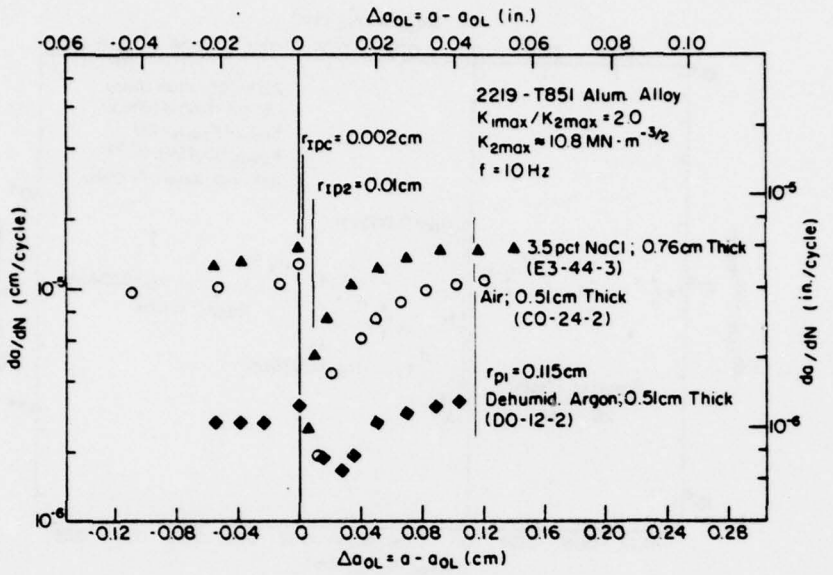

(a)

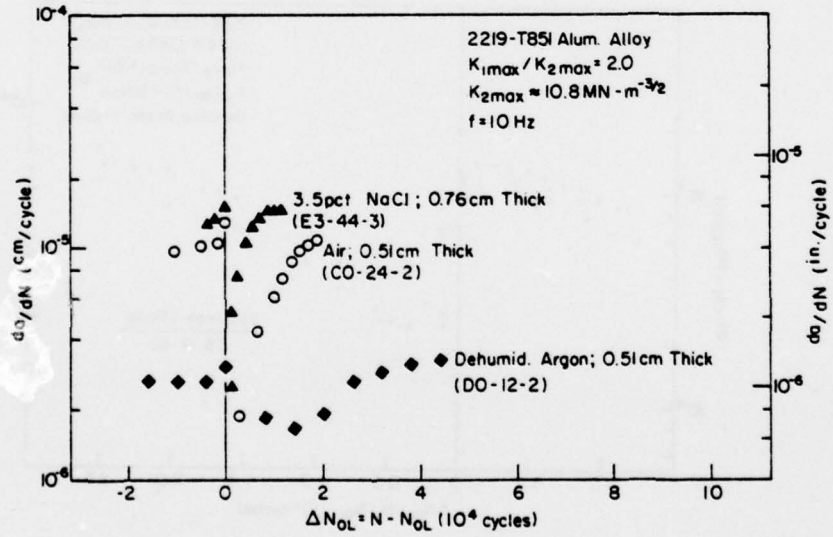

(b)

Figure 10: The influence of chemical environment on the room temperature fatigue crack growth response following a single overload at K_{1max}/K_{2max} = 2.0, with $K_{2max} \approx$ 10.8 MN-m-3/2 and R = 0.05: (a) da/dN versus Δa_{OL}, and (b) da/dN versus ΔN_{OL}.

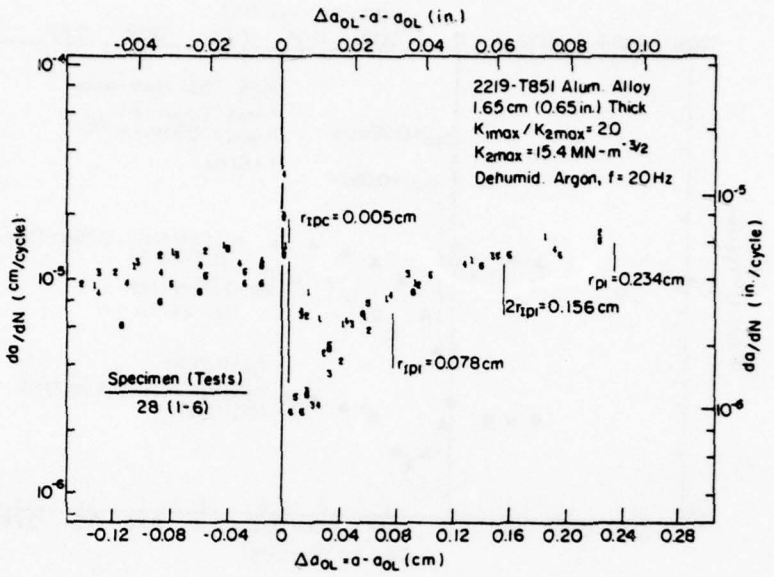

(a)

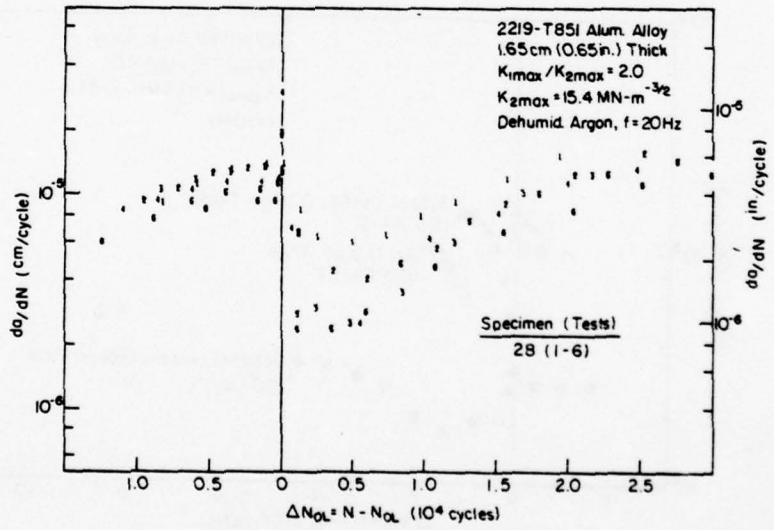

(b)

Figure 11: Fatigue crack growth response for a 1.65 cm thick specimen following a single overload at K_{1max}/K_{2max} = 2.0 and K_{2max} = 15.4 MN-m-3/2 using the "constant K" procedure: (a) da/dN versus Δa_{OL}, and (b) da/dN versus ΔN_{OL}. (Test environment: dehumidified argon at room temperature. Fatigue loading at R = 0.05).

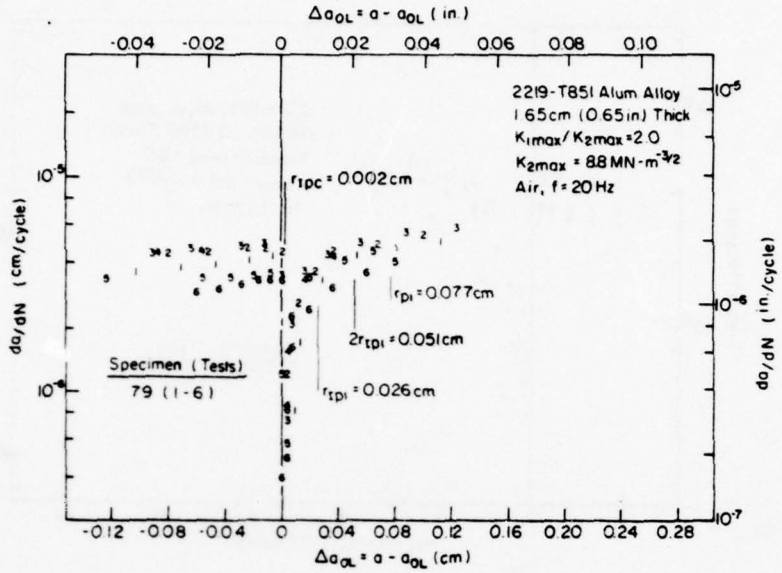

(a)

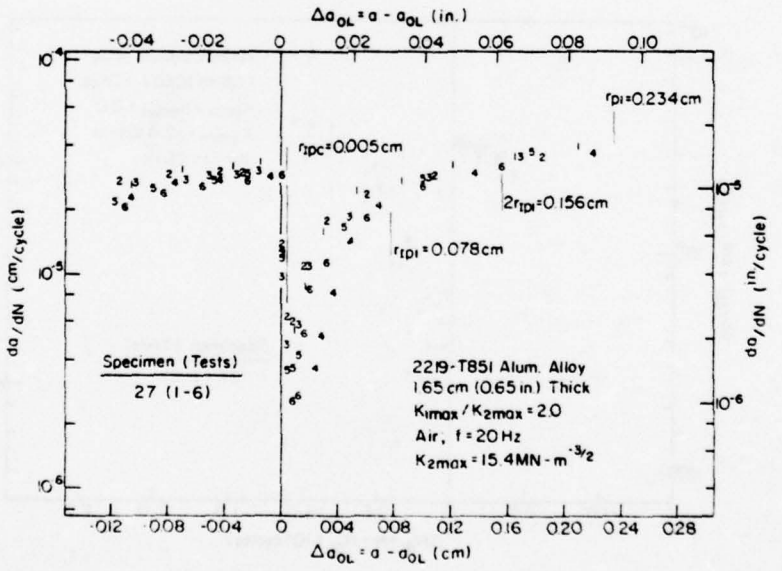

(b)

Figure 12: Fatigue crack growth response (da/dN versus Δa_{OL}) for a 1.65 cm thick specimen following a single overload at K_{1max}/K_{2max} = 2.0 using the "constant K" procedure: (a) K_{2max} = 8.8 MN-m$^{-3/2}$, and (b) K_{2max} = 15.4 MN-m-3/2. (Test environment: air at room temperature. Fatigue loading at R = 0.05).

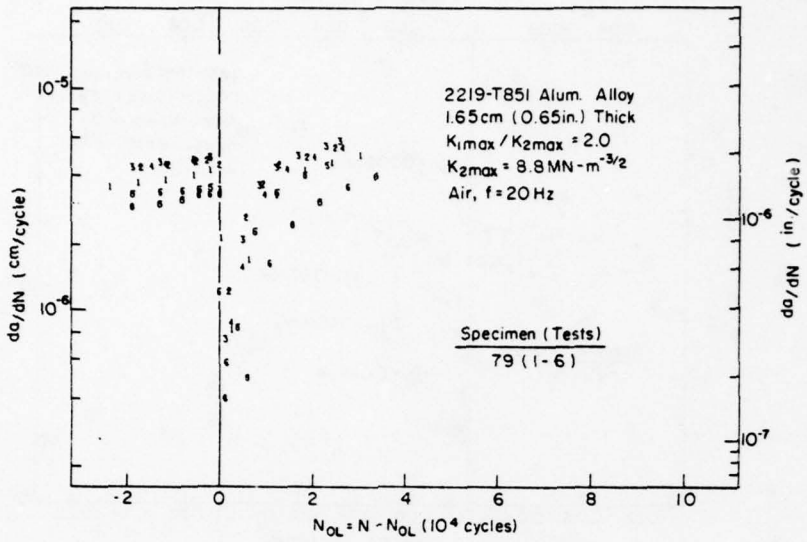

(a)

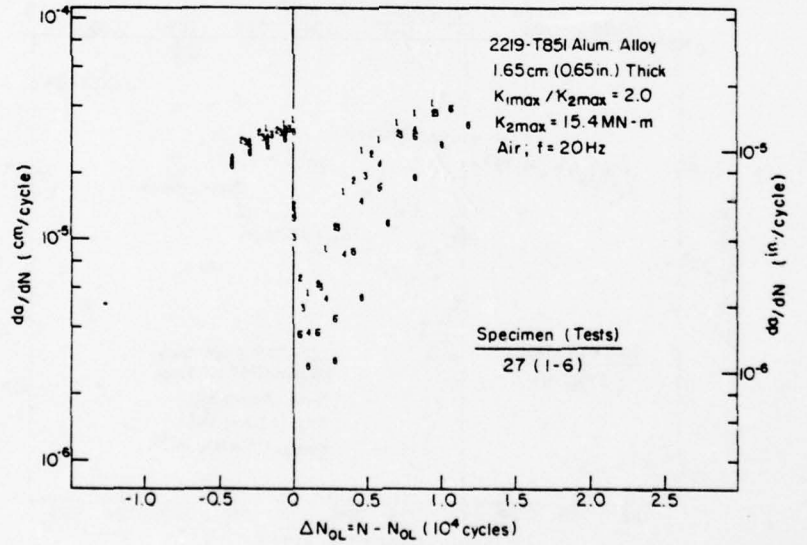

(b)

Figure 13: Fatigue crack growth response (da/dN versus ΔN_{OL}) for a 1.65 cm thick specimen following a single overload at K_{1max}/K_{2max} = 2.0 using the "constant K" procedure: (a) K_{2max} = 8.8 MN-m-3/2, and (b) K_{2max} = 15.4 MN-m-3/2. (Test environment: air at room temperature. Fatigue loading at R = 0.05).

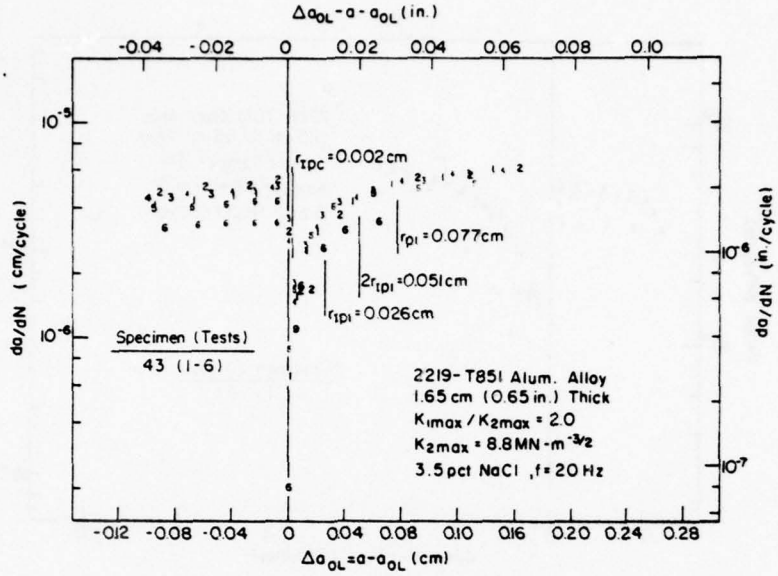

(a)

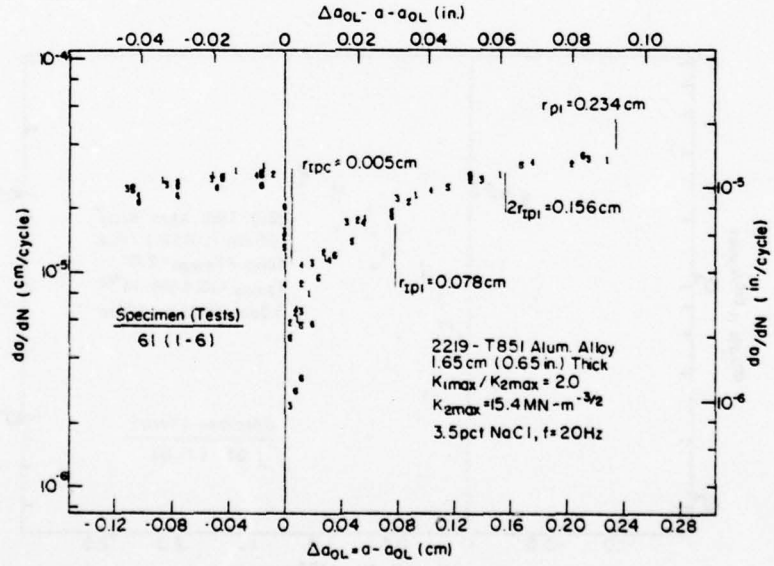

(b)

Figure 14: Fatigue crack growth response (da/dN versus Δa_{OL}) for a 1.65 cm thick specimen following a single overload at K_{1max}/K_{2max} = 2.0 using the "constant K" procedure: (a) K_{2max} = 8.8 MN-$m^{-3/2}$, and (b) K_{2max} = 15.4 MN-$m^{-3/2}$. (Test environment: 3.5 pct NaCl solution at room temperature. Fatigue loading at R = 0.05).

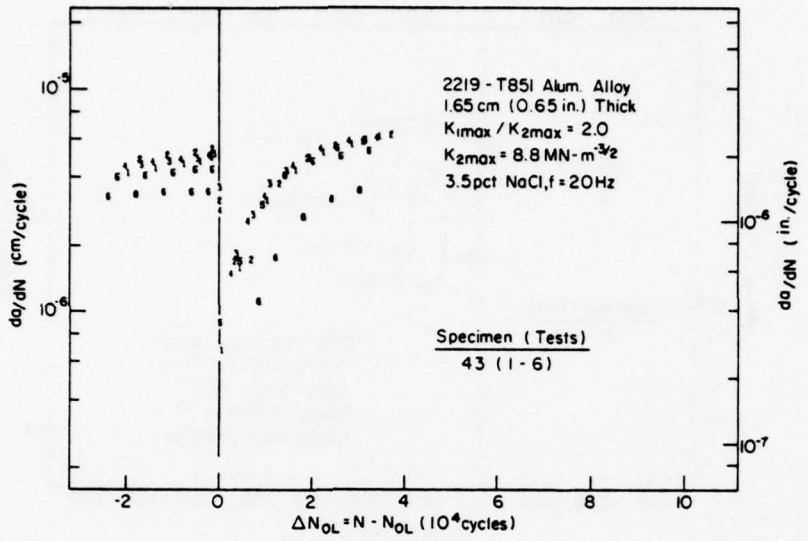

(a)

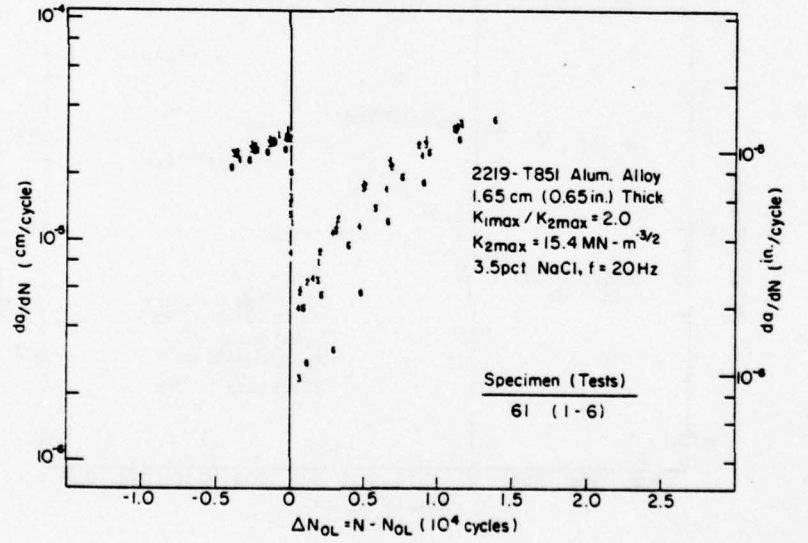

(b)

Figure 15: Fatigue crack growth response (da/dN versus ΔN_{OL}) for a 1.65 cm thick specimen following a single overload at K_{1max}/K_{2max} = 2.0 using the "constant K" procedure: (a) K_{2max} = 8.8 MN-m$^{-3/2}$, and (b) K_{2max} = 15.4 MN-m-3/2. (Test environment: 3.5 pct NaCl solution at room temperature. Fatigue loading at R = 0.05).

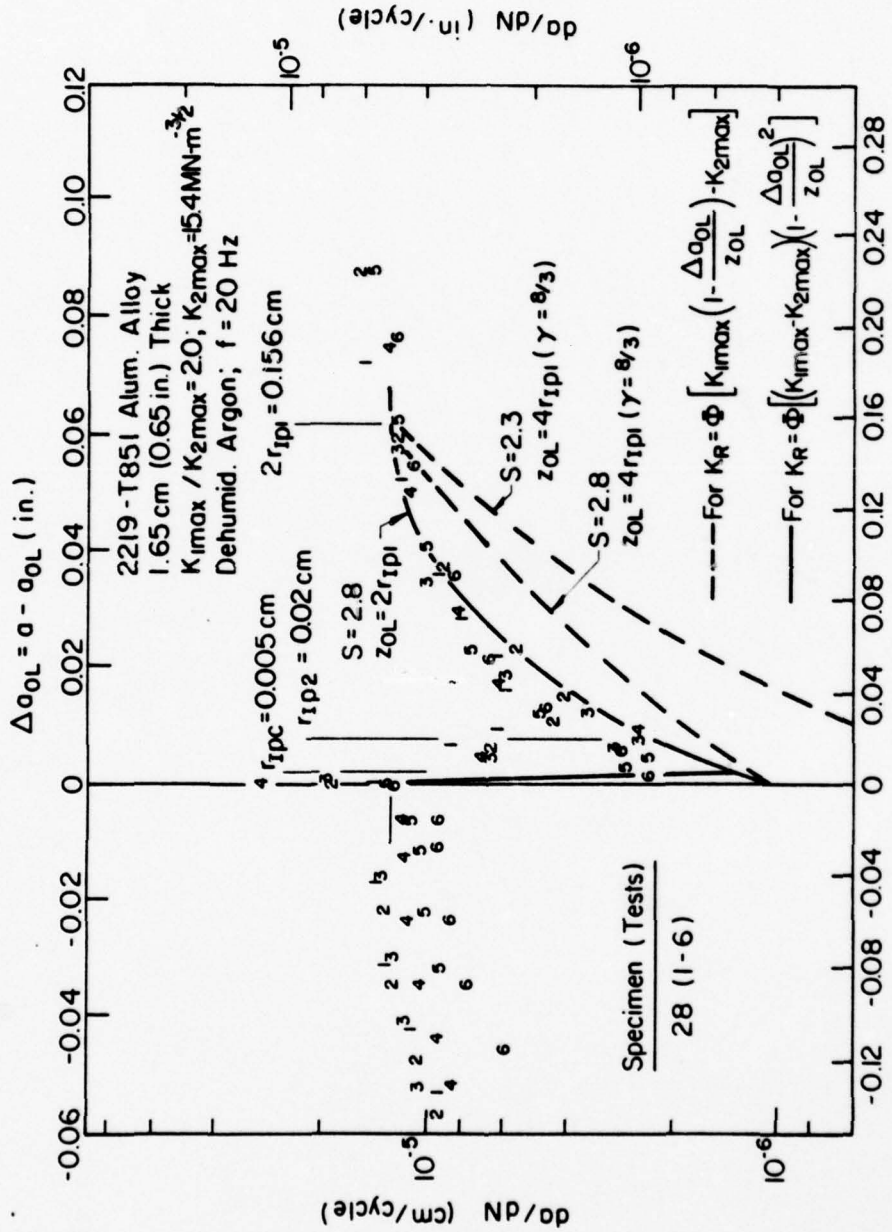

Figure 16: Comparison of fatigue crack growth response with "predictions" based on residual stress intensity factor concept.

APPENDIX B

CONSIDERATIONS OF MEASUREMENT PRECISION AND DATA PROCESSING PROCEDURES FOR FATIGUE CRACK GROWTH TESTING AND ANALYSIS

CONSIDERATIONS OF MEASUREMENT PRECISION AND DATA PROCESSING PROCEDURES FOR FATIGUE CRACK GROWTH TESTING AND ANALYSIS

by

R. P. Wei and W. Wei*
LEHIGH UNIVERSITY
Bethlehem, Pennsylvania 18015

ABSTRACT

A computer simulation of the primary fatigue crack growth data (crack length versus elapsed cycles or a versus N) was made to examine the influences of crack length measurement interval and precision, and of the associated data processing procedure on the resulting data on fatigue crack growth kinetics (i.e., da/dN versus ΔK). Variability in the derived growth rate (da/dN) data depended strongly on the magnitude of the measurement interval relative to the measurement precision. It was reduced by those data processing procedures (such as the incremental polynomial methods) that fitted a smooth curve through portions of the primary data. Such procedures, however, introduced significant bias into the derived data on fatigue crack growth kinetics. The results further suggested that much of the variability in the published data on fatigue crack growth kinetics might be attributed to sources described herein. Caution is, therefore, recommended in attempting to draw statistical inferences regarding material variability from these data.

---

*Now Research Assistant in the Department of Metallurgy and Mining Engineering, University of Illinois at Urbana-Champaign, Urbana, Illinois 61801.

INTRODUCTION

Many engineering structures are subjected to cyclically varying (fatigue) loads during service. Fatigue analysis, or the estimation of fatigue lives of such structures, is therefore an essential part of engineering design. Fracture mechanics technology [1-5], developed over the past twenty years, is well established as an important tool for fatigue crack growth analysis and for the analysis of related structural reliability problems. Standardized test methods have been, or are being, developed to obtain supporting experimental data for these analyses (for example, [6,7]). For fatigue crack growth, a typical design sequence would involve the following steps [5] which are illustrated schematically in Figure 1:

1. The acquisition of fatigue crack growth data (crack length versus number of elapsed cycles, or a vs. N) from laboratory specimens or from model components.
2. Processing these data to convert them into fatigue crack growth rate (da/dN or $\Delta a/\Delta N$) as a function of the mechanical driving force. The mechanical driving force is characterized by the fracture mechanics parameters ΔK or K_{max} (where ΔK and K_{max} are the stress intensity factor range and maximum stress intensity factor, respectively, for a given load cycle [1,2], and are functions of the applied load and current crack length [5,7].
3. Modeling or expressing the fatigue crack growth kinetics (i.e., the da/dN vs. ΔK or K_{max} data) by an

appropriate analytical or empirical relationship.

4. Utilizing the analytical or empirical relationship thus derived to predict or estimate the fatigue crack growth response for the structure and the expected service conditions of interest.

As a part of the prediction procedure, an estimate of structural reliability would be required. This estimate is provided through an estimate of the probable variations in fatigue lives or the probability for survival following a given period of service. Thus, it is important to incorporate into the analyses the variability in fatigue crack growth rate data and estimates of the accuracy of various analysis steps. Variability in fatigue data arises from several sources: (a) inherent variations in material properties (particularly its fatigue crack growth resistance), (b) variations in loading and environmental conditions during testing, and (c) variations introduced by crack length measurement precision and the associated data processing procedures. Unfortunately, however, variability introduced by these several sources are not clearly recognized and reported separately along with the kinetic data on fatigue crack growth. As a result, it is commonly (though incorrectly) assumed that the observed scatter in the kinetic data resulted principally from material property variations, and an upper-bound curve to these data is often used for design analyses [4]. This assumption, however, cannot be fully justified, because the fatigue data are often obtained from a small number of specimens; often taken from a single plate of material. Hence, the data can reflect, at best, local

variations in material properties, and do not contain the type of statistical information (in terms of heat-to-heat or plate-to-plate variations) that would be required for design.

In this investigation, variability in fatigue crack growth rate data, introduced by crack length measurement interval and precision and by the associated data processing procedures, was examined systematically through computer simulation. This investigation expanded upon preliminary studies by Clark and Hudak [4] and by Graham [8] on the effects of data processing procedure on variability. The possible influence of data processing procedures on the accurate representation of fatigue crack growth kinetics (i.e., in introducing bias) was also examined. Information from this investigation, in conjunction with assessments of the influences of loading and environmental variables through the usual error analysis procedures [9], would provide a basis for deducing variability introduced by material property variations (the requisite quantity) from the experimental fatigue data.

PROCEDURE

Because the primary experimental fatigue crack growth (a vs. N) data would contain contributions from measurement precision, as well as the effects of possible variations in material and of loading and environmental variables, it was not practicable to utilize such data to assess the influences of measurement precision and of the associated data processing procedures. If it were possible to exclude all other effects, the assessment procedure would have involved reconstruction of the fatigue crack growth

(a vs. N) curve (by following steps 1 through 4 described previously and illustrated in Figure 1) and comparison of this curve with the original crack growth data. Since this was not possible, an alternative procedure, first suggested by Clark and Hudak [4], was used. In this procedure, an analytical relationship was assumed for the fatigue crack growth kinetics. For simplicity, a simple exponential relationship was assumed to apply over the entire range of crack lengths of interest [4,10].

$$da/dN = C(\Delta K)^n \qquad (1)$$

C and n are constants (normally to be determined experimentally).[1/] An "error free" fatigue crack growth (a vs. N) curve was then created from this kinetic relationship by integrating Equation (1) between selected initial and final crack lengths. From this curve, an "error free" a vs. N data set is produced based on the chosen crack length measurement interval (Δa). Appropriate random measurement errors were then generated by computer simulation (for a prescribed measurement precision) and were applied to the "error free" a vs. N data set to produce a set of simulated fatigue crack growth (a vs. N) data. The simulated primary (a vs. N) data were then processed by the various data processing procedures to determine the fatigue crack growth kinetics. The resulting kinetic (derived) data were finally used to assess variability introduced by the choice of measurement intervals and

---

[1/] Note that C is a dimensioned constant, whose value and dimension change with n to provide growth rate in terms of length per cycle.

measurement precision.[2/] Least squares error procedure was also used to fit the derived kinetic data to an equation of the form given by Equation (1). The constants C and n determined from this procedure were then compared with the original C and n values to determine how well these values were reconstructed, and also compared amongst the different methods to test for possible bias. In essence, this alternate procedure used step 3 (illustrated in Figure 1) as a starting point, and then proceeded through steps 4, 1 and 2 to return to step 3. By this simulation procedure, the effects of measurement precision were isolated for study.

A compact specimen [7], having a width of 2.0 in., was used as a model for this investigation. The constants C and n were assumed to be $C = 4 \times 10^{-9}$ (in./cycle)(ksi-in.$^{1/2}$)$^{-n}$ and $n = 2.25$ (see Equation (1)) [4]. Simulated crack growth ranged from 0.6 to 1.6 in. Stress intensity factor solution and other details for this specimen are given in [7]. (Note that 1 ksi-in.$^{1/2}$ $\approx$ 1.1 MN-m$^{-3/2}$, and 1 in. = 2.54 cm.)

Unlike Clark and Hudak [4], who made a simplifying assumption that the measurement error was constant in magnitude and varied alternately in sign between successive measurement points, measurement error was assumed to vary randomly both in magnitude and in sign in this investigation. The measurement error was assumed to be described by a normal distribution function with a

---

[2/] Note that measurement precision would affect both da/dN and ΔK. The values of ΔK would be altered by less than 1 pct, however, in a typical experiment, and need not be considered as statistically varying quantities in the analyses.

mean of zero and a known (prescribed) standard deviation, σ. Measurement error for each successive measurement point was selected from this distribution with the aid of a random number generator. Its magnitude was rounded to a value nearest to the assumed resolution of the measurement instrument; viz., to 0.4σ.[3] The error assignment procedure is illustrated in Figure 2. By this procedure, a more realistic simulation of the random experimental errors was achieved.

The following measurement intervals and measurement precision (given in terms of σ) were selected for study. The measurement intervals are typical of those in common use and are given in English units here. (Note that 1 in. = 2.54 cm).

Interval Δa	Precision σ
0.050 in.	0.010, 0.005 and 0.0025 in.
0.025 in.	0.005, 0.0025 and 0.00125 in.
0.010 in.	0.002 and 0.001 in.

For each combination of crack length measurement interval and precision, ten different simulated fatigue crack growth (a,N) data sets were generated to provide sufficient information for statistical analysis. The different data sets were produced by using randomly selected numbers as "seeds" for the random number generator, and simulated, for example, data that might be obtained from testing 10 ideally identical specimens by a single

[3] When an infrequent error of greater than 2σ was indicated, a value equal to 2σ was assigned.

experimenter or observations of 10 different experimenters for a single specimen.

For this investigation, the variability factors VF and VF*, defined by Clark and Hadak [4,6], were adopted for measuring variability in the data on fatigue crack growth kinetics. VF provided a measure of data scatter about a least-squares-error curve through the derived data (of the form given by Equation (1); that is, using the derived values for C and n), whereas VF* provided a measure of scatter against the original curve. VF is defined by the following relationship [4,6].

$$VF = e^{4R} \tag{2}$$

R is the residual standard error defined as follows:

$$R = \left[\frac{\sum_i [\ell n(da/dN)_i - \ell n(d\hat{a}/dN)_i]^2}{Z - 2}\right]^{1/2} \tag{3}$$

where

$(da/dN)_i$ = "measured" crack growth rate at ΔK_i;

$(d\hat{a}/dN)_i$ = "predicted" crack growth rate at ΔK_i, based on the least-squares-error fit;

Z = number of data pairs; that is $(da/dN)_i$ and ΔK_i pairs.

VF* is similarly defined, except $(d\hat{a}/dN)_i$ would be given by the original constants C and n.

To examine the influences of crack length measurement interval and precision, and of the associated data processing procedures on variability, two data processing procedures that are in common usage were used [6,7]. The first procedure is the finite

difference (or secant) method. The crack growth rate was obtained by simply taking the growth increment between two adjacent points and dividing it by the number of elapsed cycles.

$$(da/dN)_i = \frac{a_{i+1} - a_i}{N_{i+1} - N_i} \tag{4}$$

The average crack length, $(a_{i+1} + a_i)/2$, was used to compute the corresponding value for ΔK_i. The second method, the seven-point incremental polynomial method, involved least-squares-error fitting of a second-order polynomial in N to seven successive (a,N) data pairs (i.e., over the range $a_{i-3} \leq a \leq a_{i+3}$). Crack growth rate was then computed as a derivative to this polynomial, along with ΔK_i, at the central (or ith) point [6,7]. The following relations were used in calculating da/dN [6,7]:

$$a = b_o + b_1 \left(\frac{N-C_1}{C_2}\right) + b_2 \left(\frac{N-C_1}{C_2}\right)^2 \tag{5}$$

$$(da/dN)_i = \frac{b_1}{C_2} + 2b_2 \frac{(N_i - C_1)}{C_2^2} \tag{6}$$

where

$$C_1 = \frac{1}{2} (N_{i-3} + N_{i+3})$$

$$C_2 = \frac{1}{2} (N_{i+3} - N_{i-3})$$

The numbers of elapsed cycles were normalized in terms of C_1 and C_2 to circumvent the need of dealing with large numbers in the least-squares-error fitting routine [4,6].

For examining the influences of data processing procedures, the incremental polynomial procedure was expanded to include 5 and

9 points. In addition, a procedure that involved fitting parabolas through 3 adjacent data points (Simpson's rule) was also included; with the computation of growth rate made again at the central point. A measurement interval of 0.025 in., with σ = 0.005 and 0.00125 in., was used in this part of the study. Each data processing procedure was used to analyze the same 10 sets of simulated (a,N) data corresponding to the chosen measurement interval and precision. Adjustments were made to ensure that the same number of ($da/dN,\Delta K$) data pairs (covering the same range of crack lengths or ΔK) was included in each procedure, and were achieved by excluding appropriate numbers of ($da/dN,\Delta K$) pairs at the beginning and at the end to yield the same number of data pairs as that of the 9-point incremental polynomial method.

Analyses of the results were made by comparing the mean values of C and n from each data processing procedure (with 10 sets for each condition) at the 95 percent confidence level [11, 12]. The statistical tests used required that each group of ten C and n values from each procedure and condition be normally distributed. All of the C and n values were assessed [11,12] and were found to satisfactorily fulfill the normality requirement in each case.

RESULTS AND DISCUSSIONS

The influences of measurement interval and precision and of the associate data processing procedures on variability, and the possible influences of the various data processing procedures in introducing bias, are reported and discussed separately.

Measurement Interval and Precision

The results obtained from an investigation of the influences of crack length measurement interval and precision and of the associated data processing procedure on variability in fatigue crack growth rates are summarized in Table 1. It can be seen that the variability (as measured by VF and VF*) decreased as the measurement precision was increased (i.e., for decreasing values of σ). For a given measurement precision (or σ), the results on variability appear to be somewhat ambiguous. For the finite difference (secant) method, the variability increased with decreasing measurement interval. For the incremental polynomial method, variability (as indicated by VF) increased with decreasing measurement interval, whereas VF* appeared to indicate improvement (from $\Delta a = 0.050$ in. to $\Delta a = 0.025$ in.) before it worsened. For a given ratio of σ to Δa (for example, at $\sigma/\Delta a = 0.1$) there appeared to be an initial slight improvement followed by little change in variability with decrease in measurement interval. One must recognize that the total number of (a,N), and the corresponding (da/dN,ΔK) data pairs increased with decreasing measurement interval; the number of (a,N) data points being 20, 40 and 100 respectively for Δa of 0.050, 0.025 and 0.010 in. in the present case. Since the variability is associated with the same population, the observed trend is to be expected.

Comparison between VF and VF* for the two data processing procedures indicated that the secant method produced greater variability. This result was expected, because the incremental polynomial method tended to "smooth out" the data. Comparison

between VF and VF*, for a given data processing procedure, indicated that VF and VF* for a given $\Delta a, \sigma$ combination were essentially equal for the secant method, whereas they were significantly different for the incremental polynomial method. The larger VF* values suggested that data did not agree with the originally assumed curve, and that the incremental polynomial method tended to introduce a systematic bias into the processed data. This observation is supported by comparing the tabulated values of C and n against the originally assumed values of $C = 4 \times 10^{-9}$ and $n = 2.25$. A more detailed evaluation of the data processing procedure is given in the following section.

Examination of VF and VF* in Table 1 (particularly for the secant method) shows that significant variability can be introduced by the injudicious choice of measurement interval in relation to the measurement precision. It appears that a measurement interval equal to 10 times the measurement precision (i.e., $\Delta a = 10\ \sigma$) would produce a "tolerable" scatter in the fatigue crack growth rate data. There is, however, an upper limit to the choice of measurement interval. This choice is dictated by the desired precision in identifying crack length and the corresponding ΔK with the measured crack growth rate. The choice of measurement interval must be based also on a realistic assessment of measurement precision (which must be established experimentally and is not the same as the smallest division on a measuring instrument -- viz. instrumental resolution -- as is often assumed). Assessment of measurement precision may be made, for example, from independent measurements of several crack specimens by different investi-

gators, or from repeated measurements of these same specimens by the same investigator, taken at random and at different times to minimize bias.

The magnitudes of the variability factors (VF and VF*) given in Tables 1 and 2 are comparable to those deduced from typical experimental data (see [6], for example). This comparison suggests that much of the scatter in the published data on fatigue crack growth kinetics may be attributed to the measurement and data processing procedures. Until variability from these sources, along with that introduced by load and environment variation during each test and from test to test, can be separated from the experimental data (obtained from sufficient numbers of specimens), no meaningful information with respect to material property variations can be deduced. One should, therefore, refrain from drawing statistical inferences with respect to material property variations directly from the experimental data on fatigue crack growth kinetics at this time.

Data Processing Procedure

C, n, VF and VF* values, along with the estimates of standard errors, are summarized in Table 2 and are given in two parts. In the first part, the values were deduced by using the same number of points (32), over the same range of crack lengths or ΔK, for each procedure. In the second part, the values were deduced from all of the data points produced by each procedure. Information from the first part was used to compare the data processing procedures against one another, and the results are summarized in

Table 3. The second part was used to compare the individual procedures against the original curve. This comparison is given in Table 4.

Statistical tests [11,12], at the 95 percent confidence level, showed that there was a systematic bias introduced by the incremental polynomial methods, as indicated by reduced values of C and increased n (see Tables 2 to 4). The bias increased with increasing number of points used in the incremental polynomial method. The finite difference (secant) method and the parabolic curve fitting procedure (Simpson's rule) did not show significant bias, although these methods produced greater scatter (see Tables 2 to 4). It appears that one of these two methods should be used for data processing, at least in a fundamental sense (for example, to try to deduce a fundamental fatigue crack growth relationship from experimental data). In a practical sense, the bias may not be significant in terms of probable errors in predicted fatigue lives. The question of practical significance needs to be established by more detailed studies covering a broad range of da/dN versus ΔK relationships and a wider range of crack lengths.

CONCLUSION

The results of this investigation indicate that considerable variability in fatigue crack growth rate data can result from the choice of crack length measurement interval in relation to the measurement precision, and the associated data processing procedures. Data processing procedures that tend to reduce scatter, through the use of "smoothing" techniques, could introduce bias

into the results. With suitable choice of measurement interval in relation to precision (viz., $\Delta a/\sigma$ = 10 to 20), data obtained by the secant method appears to best represent actual response, with an acceptable degree of variability (i.e., VF $\leq$ 2). One must be realistic, however, in assessing the measurement precision.

These results further suggested that much of the variability in the published data on fatigue crack growth kinetics might be attributed to sources described herein. Caution is, therefore, recommended in attempting to draw statistical inferences regarding material variability from these data.

ACKNOWLEDGEMENT

The authors express their sincere appreciation to Professor Sutton Monro of Lehigh University and Dr. Gary A. Miller of Bethlehem Steel Corporation for their many helpful discussions and their critical review of this manuscript. Support of this work by the Air Force Office of Scientific Research under Grant AFOSR-75-2857 is gratefully acknowledged.

REFERENCES

1. Paris, P. C., in Fatigue - An Interdisciplinary Approach, Syracuse University Press, 1964, p. 107.

2. McEvily, A. J. and Wei, R. P., in Corrosion Fatigue: Chemistry, Mechanics and Microstructure, NACE-2, 1972, p. 381.

3. Gallagher, J. P. and Stalnaker, H. D., Journal of Aircraft, Vol. 12, No. 9, 1975, p. 699.

4. Clark, W. G., Jr. and Hudak, S. J., Jr., "The Analysis of Fatigue Crack Growth Rate Data", in Application of Fracture Mechanics to Design, Syracuse University Press (to be published).

5. Wei, R. P., "Fracture Mechanics Approach to Fatigue Analysis in Design", Journal of Engineering Materials and Technology, ASME, (to be published).

6. Clark, W. G., Jr. and Hudak, S. J., Jr., Journal of Testing and Evaluation, JTEVA, Vol. 3, No. 6, 1975, p. 454.

7. "Tentative Method of Test for Constant-Load-Amplitude Fatigue Crack Growth Rates above 10^{-8} m/cycle", ASTM, 1977. (Note that this tentative method is in the approval process).

8. Graham, J. A., unpublished results, Lehigh University, 1976.

9. Rabinowicz, E., An Introduction to Experimentation, Addison-Wesley, Reading, Mass., 1970.

10. Paris, P. C. and Erdogan, F., Journal of Basic Engineering, ASME, Vol. 85, 1963, p. 528.

11. Guttman, I., Wilks, S. S. and Hunter, J. S., Introductory Engineering Statistics, 2nd edition, John Wiley & Sons, New York, 1971.

12. Hald, A., Statistical Theory with Engineering Applications, John Wiley & Sons, New York, 1952.

Table 1: Summary of Influences of Crack Length Measurement Interval and Precision on Fatigue Crack Growth Data for Two Data Processing Procedures

Measurement		Secant Method								7-Point Incremental Polynomial Method							
Interval Δa (in.)	Precision σ (in.)	$Cx10^9$		n		VF		VF*		$Cx10^9$		n		VF		VF*	
		Avg.	s	Avg.	s	Avg.	s	Avg.	s	Avg.	s	Avg.	s	Avg.	s	Avg.	s
0.050	0.010	4.58	1.43	2.21	0.081	4.16	1.19	4.20	1.22	3.72	0.74	2.29	0.056	1.22	0.05	1.48	0.10
	0.005	4.10	0.48	2.24	0.032	1.95	0.23	1.96	0.25	3.43	0.31	2.31	0.026	1.13	0.04	1.40	0.06
	0.0025	4.02	0.17	2.25	0.012	1.36	0.06	1.36	0.05	3.43	0.15	2.31	0.012	1.05	0.02	1.37	0.02
0.025	0.005	3.81	0.54	2.25	0.038	3.89	0.43	3.98	0.46	3.62	0.17	2.28	0.012	1.21	0.04	1.25	0.04
	0.0025	3.96	0.21	2.25	0.014	1.73	0.09	1.74	0.09	3.66	0.10	2.28	0.007	1.10	0.02	1.15	0.02
	0.00125	4.02	0.10	2.25	0.007	1.34	0.05	1.35	0.05	3.65	0.05	2.28	0.004	1.04	0.01	1.13	0.01
0.010	0.002	3.79	0.37	2.25	0.023	3.65	0.41	3.71	0.44	3.94	0.07	2.26	0.005	1.16	0.02	1.16	0.02
	0.001	4.02	0.11	2.25	0.007	1.74	0.07	1.75	0.07	3.97	0.03	2.25	0.002	1.08	0.01	1.08	0.01

Note: The average and standard error values for C, n, VF and VF* are based on 10 sets of data. Initially assumed values for C and n were $C=4x10^{-9}$ $(in./cycle)(ksi\sqrt{in.})^{-2.25}$ and n = 2.25.

Table 2: The Influence of Data Processing Procedure on Fatigue Crack Growth Data

Data Processing Methods	Δa=0.025 in., σ=0.005 in.								Δa=0.025 in., σ=0.00125 in.							
	$Cx10^9$		n		VF		VF*		$Cx10^9$		n		VF		VF*	
	Avg.	s	Avg.	s	Avg.	s	Avg.	s	Avg.	s	Avg.	s	Avg.	s	Avg.	s
A1	3.49	0.19	2.30	0.015	1.15	0.04	1.24	0.04	3.53	0.06	2.29	0.004	1.03	0.008	1.19	0.006
B1	3.60	0.23	2.29	0.018	1.21	0.04	1.25	0.05	3.66	0.07	2.28	0.005	1.04	0.009	1.12	0.007
C1	3.76	0.30	2.27	0.022	1.36	0.05	1.37	0.05	3.82	0.07	2.27	0.005	1.07	0.010	1.09	0.010
D1	3.89	0.45	2.26	0.032	1.91	0.14	1.92	0.14	3.94	0.09	2.25	0.006	1.16	0.022	1.16	0.023
E1	3.75	0.60	2.26	0.041	3.91	0.61	3.99	0.64	3.99	0.16	2.25	0.011	1.35	0.064	1.35	0.064
A2	3.49	0.19	2.30	0.015	1.15	0.04	1.24	0.04	3.53	0.06	2.29	0.004	1.03	0.008	1.19	0.006
B2	3.62	0.17	2.28	0.012	1.21	0.04	1.25	0.04	3.65	0.05	2.28	0.004	1.04	0.009	1.13	0.008
C2	3.79	0.19	2.27	0.013	1.35	0.04	1.36	0.04	3.80	0.06	2.27	0.004	1.07	0.009	1.09	0.010
D2	3.96	0.31	2.25	0.020	1.89	0.11	1.90	0.11	3.96	0.08	2.25	0.006	1.16	0.020	1.16	0.020
E2	3.81	0.54	2.25	0.038	3.89	0.43	3.98	0.46	4.02	0.10	2.25	0.007	1.34	0.047	1.35	0.047

Note 1: See note for Table 1.
Note 2: Method A: 9-point incremental polynomial method.
Method B: 7-point incremental polynomial method.
Method C: 5-point incremental polynomial method.
Method D: Simpson's rule (3-point parabolic fit).
Method E: Secant method.
1 = Same number of data points as Method A; 2 = all data points.

Table 3: Statistical Comparison of C and n Values from Different Data Processing Methods Using the Same Number of Processed Data Pairs (see Table 2).

Measurement Interval and Precision	C/n	C[1]					n[1]				
	Methods[2]	A1	B1	C1	D1	E1	A1	B1	C1	D1	E1
Δa=0.025 in. σ=0.005 in.	A1	I	E	L	L	E	I	E	G	G	G
	B1	E	I	E	L	E	E	I	G	G	G
	C1	G[3]	E	I	E	E	L	L	I	E	E
	D1	G	G	E	I	E	L	L	E	I	E
	E1	E	E	E	E	I	L	L	E	E	I
Δa=0.025 in. σ=0.00125 in.	A1	I	L	L	L	L	I	G	G	G	G
	B1	G	I	L	L	L	L	I	G	G	G
	C1	G	G	I	L	L	L	L	I	G	G
	D1	G	G	G	I	E	L	L	L	I	E
	E1	G	G	G	E	I	L	L	L	E	I

(1) See Note for Table 1.

(2) See Note for Table 2.

(3) E = equal to, L = less than and G = greater than on a 95 percent confidence basis. For example, C for the 5-point incremental polynomial method (C1) is greater than that for the 9-point incremental polynomial method (A1) at the 95 percent confidence level. I = identity.

Table 4: Statistical Comparison of C and n Values from Different Data Processing Methods with the Initially Assumed Values (see Table 2).

Measurement Interval and Precision	Δa=0.025 in., σ=0.005 in.		Δa=0.025 in., σ=0.00125 in.	
Methods	$C=4 \times 10^{-9}$	n=2.25	$C=4 \times 10^{-9}$	n=2.25
A1	L	G	L	G
B1	L	G	L	G
C1	L	G	L	G
D1	E	E	L	G
E1	E	E	E	E
A2	L	G	L	G
B2	L	G	L	G
C2	L	G	L	G
D2	E	E	E	E
E2	E	E	E	E

See notes for Tables 1, 2 and 3. L, E and G indicate that the processed C and n values are less than, equal to or greater than the initially assumed values of C and n, respectively, at the 95 percent confidence level.

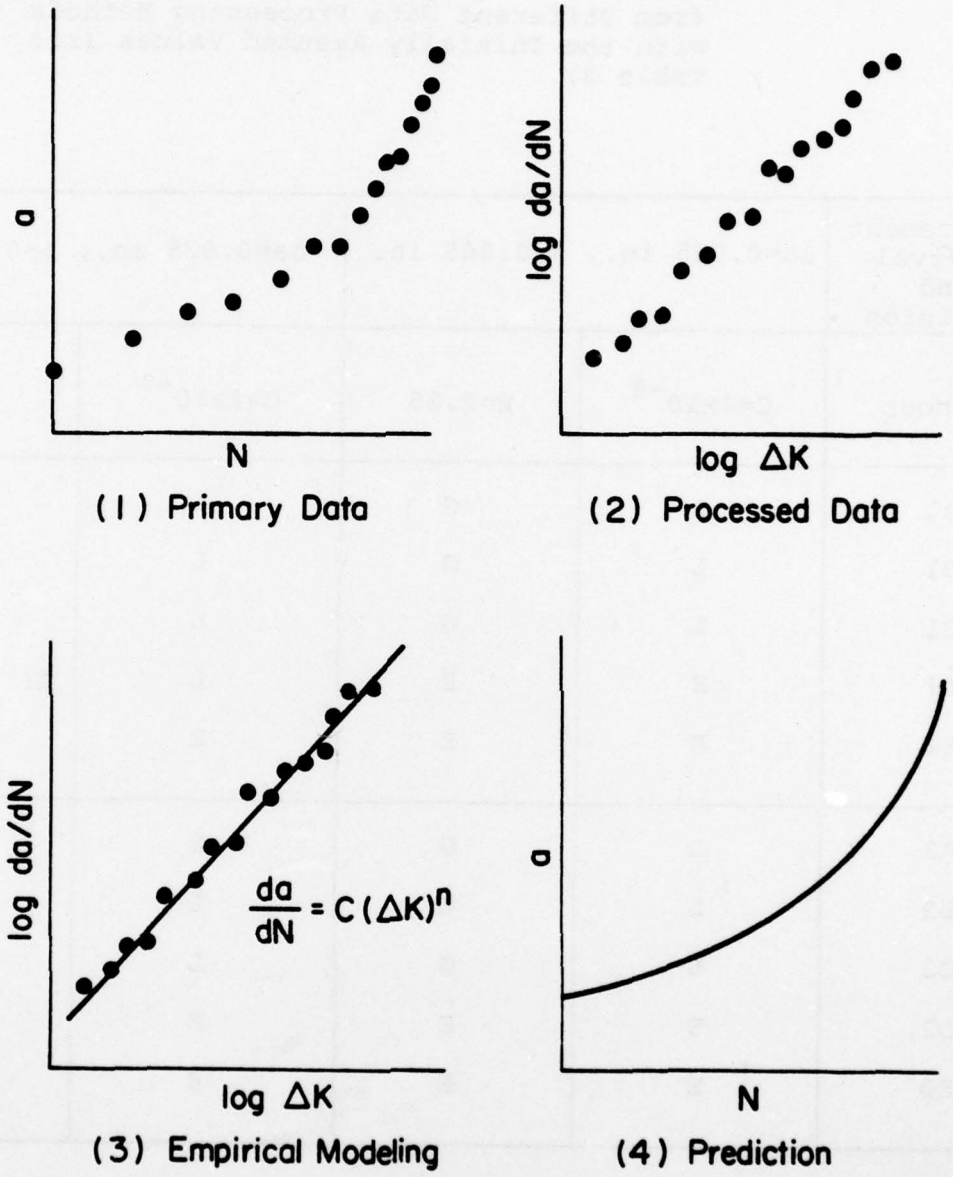

Figure 1: Schematic illustration of the sequential steps involved in fatigue crack growth analysis for design.

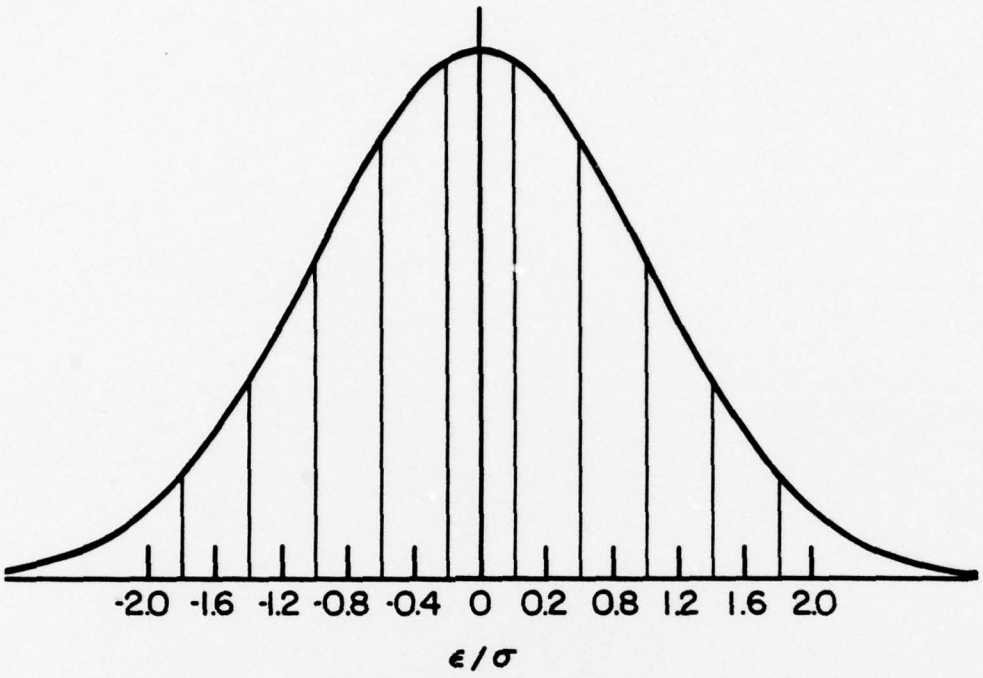

Random Number	Error Assignment
$m < 0.0359$	$\varepsilon = -2.0\sigma$
$0.0359 \leq m < 0.0808$	$\varepsilon = -1.6\sigma$
$0.0808 \leq m < 0.1587$	$\varepsilon = -1.2\sigma$
$0.1587 \leq m < 0.2743$	$\varepsilon = -0.8\sigma$
$0.2743 \leq m < 0.4207$	$\varepsilon = -0.4\sigma$
$0.4207 \leq m < 0.5793$	$\varepsilon = 0$
$0.5793 \leq m < 0.7257$	$\varepsilon = +0.4\sigma$
$0.7257 \leq m < 0.8413$	$\varepsilon = +0.8\sigma$
$0.8413 \leq m < 0.9192$	$\varepsilon = +1.2\sigma$
$0.9192 \leq m < 0.9641$	$\varepsilon = +1.6\sigma$
$0.9641 < m$	$\varepsilon = +2.0\sigma$

Figure 2: Illustration of procedure for assigning measurement error.

~~UNCLASSIFIED~~
SECURITY CLASSIFICATION OF THIS PAGE (When Data Entered)

(14) IFSM-78-88

REPORT DOCUMENTATION PAGE

READ INSTRUCTIONS BEFORE COMPLETING FORM

(18) 1. REPORT NUMBER: AFOSR-TR-78-0788

2. GOVT ACCESSION NO.

3. RECIPIENT'S CATALOG NUMBER

(6) 4. TITLE (and Subtitle)

LOAD AND ENVIRONMENT INTERACTIONS IN FATIGUE CRACK GROWTH UNDER SPECTRUM LOADING.

(9) 5. TYPE OF REPORT & PERIOD COVERED: FINAL rept. 15 Jun 75 - 30 Sep 77,

6. PERFORMING ORG. REPORT NUMBER: IFSM-78-88

(10) 7. AUTHOR(s): R. P. WEI

(15) 8. CONTRACT OR GRANT NUMBER(s): AFOSR-75-2857

9. PERFORMING ORGANIZATION NAME AND ADDRESS
LEHIGH UNIVERSITY
INSTITUTE OF FRACTURE & SOLID MECHANICS
BETHLEHEM, PA 18015

(16) 10. PROGRAM ELEMENT, PROJECT, TASK AREA & WORK UNIT NUMBERS: 2307B2 (17) B2
61102F

11. CONTROLLING OFFICE NAME AND ADDRESS
AIR FORCE OFFICE OF SCIENTIFIC RESEARCH/NA
BLDG 410
BOLLING AIR FORCE BASE, D C 20332

(11) 12. REPORT DATE: Jan 78 (12) 25p.

13. NUMBER OF PAGES: 77

14. MONITORING AGENCY NAME & ADDRESS (if different from Controlling Office)

15. SECURITY CLASS. (of this report): UNCLASSIFIED

15a. DECLASSIFICATION/DOWNGRADING SCHEDULE

16. DISTRIBUTION STATEMENT (of this Report)

Approved for public release; distribution unlimited.

17. DISTRIBUTION STATEMENT (of the abstract entered in Block 20, if different from Report)

18. SUPPLEMENTARY NOTES

19. KEY WORDS (Continue on reverse side if necessary and identify by block number)

FRACTURE MECHANICS
FATIGUE CRACK GROWTH
ALUMINUM ALLOY
CRACK CLOSURE
THICKNESS EFFECT
STRESS RATIO EFFECT
ENVIRONMENTAL EFFECT
RETARDATION
LOAD INTERACTION

20. ABSTRACT (Continue on reverse side if necessary and identify by block number)

The importance of delay (or, retardation in the rate of fatigue crack growth)produced by load interactions in variable-amplitude loading on the accurate prediction of fatigue lives of aircraft and other engineering structures has been recognized for some time and has begun to receive greater attention in recent years. Recent investigations showed that the effects of delay can be quite large, and that these effects need to be taken into accoun in developing improved fatigue analysis procedures for aircraft and other engineering structures. A number of models (based on the concepts of crack closure, residual stress, residual stress intensity factor, etc.) have been proposed to account for the

DD FORM 1 JAN 73 1473 EDITION OF 1 NOV 65 IS OBSOLETE

UNCLASSIFIED

407 099

effects of delay. These models, while successfully predicting trends in the rate of fatigue crack growth for randomized load spectra, appear to break down for ordered spectra. Several basic problems contributed to the lack of complete success, and needs to be resolved in the development of improved models for prediction load interaction effects (chiefly delay) on fatigue crack growth. They are: o Proper characterization and physical understanding of the complex phenomena of crack acceleration and delay associated with changes in load level, and of the effects of thermal and chemical environments on these phenomena. o Adequate description of crack tip stress intensity factors to account for various types of loading, crack geometry and residual stresses. o Proper description of the kinetics of fatigue crack under constant-amplitude loading, including the effects of stress ratio, cyclic load frequency and service environment, and assessment of variability in these kinetic data. To address some of the issues, the following three investigations were carried out under this grant: (1) Experimental evaluation of crack closure and its viability as a model for describing fatigue crack growth kinetics and delay. (2) Examinations of the influences of plate thickness, K level and chemical environment on fatigue crack growth response following a single high-load excursion (overload) to develop further phenomenological understanding of load interaction effeects in fatigue. (3) Assessment of the contributions of crack length measurement interval and precision, and data processing procedures on variability to provide background for interpretation of experimental data on fatigue crack growth kinetics and their utilization in life prediction. Results from these investigations are summarized. These results provide additional insight into load and environment interactions in fatigue crack growth under variable-amplitude (spectrum) loading, should be considered in assessing current life prediction procedures and in the development of improved prediction procedures.